Miner Petrol (2011) 101:21–48
DOI 10.1007/s00710-010-0136-4

ORIGINAL PAPER

Geochemical, zircon U–Pb dating and Sr–Nd–Hf isotopic constraints on the age and petrogenesis of an Early Cretaceous volcanic-intrusive complex at Xiangshan, Southeast China

Shui-Yuan Yang · Shao-Yong Jiang · Yao-Hui Jiang · Kui-Dong Zhao · Hong-Hai Fan

Received: 22 January 2010 / Accepted: 30 September 2010 / Published online: 20 October 2010

Abstract The Late Mesozoic geology of Southeast China is characterized by extensive Jurassic to Cretaceous magmatism consisting predominantly of granites and rhyolites and subordinate mafic rocks, forming a belt of volcanic-intrusive complexes. The Xiangshan volcanic-intrusive complex is located in the NW region of the belt and mainly contains the following lithologies: rhyodacite and rhyodacitic porphyry, porphyritic lava, granite porphyry with mafic microgranular enclaves, quartz monzonitic porphyry, and lamprophyre dyke. Major and trace-element compositions, zircon U–Pb dating, and Sr–Nd–Hf isotopic compositions have been investigated for these rocks. The precise SHRIMP and LA–ICP–MS zircon U–Pb dating shows that the emplacement of various magmatic units at Xiangshan took place within a short time period of less than 2 Myrs. The stratigraphically oldest rhyodacite yielded a zircon U–Pb age of 135±1 Ma and the overlying rhyodacitic porphyry has an age of 135±1 Ma. Three porphyritic lava samples yielded zircon U–Pb ages of 136±1 Ma, 132±1 Ma, and 135±1 Ma, respectively. Two subvolcanic rocks (granite porphyry) yielded zircon U–Pb ages of 137±1 Ma and 137±1 Ma. A quartz monzonitic porphyry dyke, which represented the final stage of magmatism at Xiangshan, also yielded a zircon U–Pb age of 136±1 Ma. All these newly obtained precise U–Pb ages demonstrate that the entire magmatic activity at Xiangshan was rapid and possibly took place at the peak of extensional tectonics in SE China. The geochemical data indicate that all these samples from the volcanic-intrusive complex have an A-type affinity. Sr–Nd–Hf isotopic data suggest that the Xiangshan volcanic-intrusive complex derived mainly from remelting of Paleo-Mesoproterozoic crust without significant additions of mantle-derived magma. However, the quartz monzonitic porphyry, which has zircon Hf model ages older than the whole-rock Nd model ages, and which has $\varepsilon_{Nd}(T)$ value higher than the other rocks, may indicate involvement of a subordinate younger mantle-derived magma in its origin. Geochemical data indicate that the various rocks show variable REE patterns and negative anomalies of Ba, Nb, Sr, P, Eu and Ti in the trace element spidergrams, suggesting that these rocks may have undergone advanced fractional crystallization with separation of plagioclase, K-feldspar and accessory minerals such as allanite. We suggest that this Cretaceous volcanic-intrusive complex formed in an extensional environment, and the formation of the Xiangshan mafic microgranular enclaves can be explained by the injection of mafic magma from a deeper seated mantle magma chamber into a hypabyssal felsic magma chamber at the crustal emplacement levels.

Editorial handling: J. Raith

S.-Y. Yang · S.-Y. Jiang (✉) · Y.-H. Jiang · K.-D. Zhao
State Key Laboratory for Mineral Deposits Research,
School of Earth Sciences and Engineering, Nanjing University,
Nanjing 210093, China
e-mail: shyjiang@nju.edu.cn

H.-H. Fan
Beijing Research Institute of Uranium Geology,
Beijing 100029, China

Introduction

During the Late Mesozoic period, extensive magmatism took place in southeast China with which economically significant W, Sn, Mo, Bi, U, Cu, Pb, Zn, Nb, Ta, REE, and Sb mineralization is genetically associated. This igneous activitiy is divided into two main age groups, the Early

Yanshanian Jurassic (180 to 140 Ma; J_2–J_3) and Late Yanshanian Cretaceous (140 to 97 Ma; K_1) (Li 2000; Zhou and Li 2000). The geodynamic setting and tectonic regime of Yanshanian magmatism is a hot topic of international interest and remains controversial. Many contrasting models are proposed: (1) Alpine-type collision between the Yangtze and Cathaysia Blocks (Hsü et al. 1988; 1990); (2) continental rifting and basin formation (Gilder et al. 1991; Li 2000); (3) subduction of the paleo-Pacific plate at an active continental margin; for the latter model mechanisms have been suggested by different researchers, including a normal continental arc (Jahn et al. 1990; Charvet et al. 1994; Martin et al. 1994; Lan et al. 1996; Lapierre et al. 1997), shallow subduction and roll-back (Zhou and Li 2000; Zhou et al. 2006), and foundering of a flat-subducting slab followed by slab roll-back (Li et al. 2007; Li and Li 2007).

Precise estimates of the onset and duration of magmatism are important not only for constraining the age relations with mineralization, but also for better understanding processes of mantle dynamics and melt generation within thinned continental crust during extension. The Xiangshan volcanic-intrusive complex, containing the largest volcanic-hosted uranium deposits in China, is located in Jiangxi Province, Southeast China. The timing and duration of the magmatism forming this complex has been controversial. Previous studies of the regionally extensive volcanic-intrusive units at Xiangshan gave a large age variation (e.g. Chen et al. 1999; Yu 2001; Fan et al. 2005; Zhang and Li 2007) and it is difficult to link the age data with information on the magma evolution of individual systems (Yang et al. 2010). Previously, the volcanic activity at Xiangshan was considered to take place mainly in the Late Jurassic and continued to the Early Cretaceous (158 to 135 Ma) (Jiang et al. 2005), and two magmatic cycles were distinguished (e.g. Xia et al. 1992; Wu 1999). Recently, ages of 135±1 Ma and 135±1 Ma were obtained for a rhyodacite and a rhyodacitic porphyry, respectively (Yang et al. 2010), indicating that the large-scale Xiangshan volcanic-intrusive activity took place in the Early Cretaceous rather than in the Late Jurassic. New data presented here indicate that the Xiangshan volcanic-intrusive activity was rather short-lived and that some of the ages obtained by previous researchers are inaccurate and need to be reinvestigated. In this study, we present precise zircon U–Pb ages, together with major and trace element and Sr–Nd–Hf isotopic data for the whole Xiangshan complex, in an attempt to better constrain the ages of the various rock types and the petrogenetic processes involved.

Geological setting

The Xiangshan intrusive-volcanic complex in Jiangxi Province, SE China, is located in the Ganhang tectonic belt (Gilder et al. 1996), a tectonic suture zone between the Yangtze and Cathaysia blocks (Fig. 1). The complex, comprising a resurgent caldera (collapsed caldera and resurgent dome association), is located at the northwest end of a zone of volcanic-intrusive complexes in SE China, and has ellipsoidal shape. The Xiangshan basin is approximately 26.5 km long and 15 km wide, covering an area of about 309 km^2. It is a large-scale volcanic collapse basin (Fig. 2), with the basement of the complex consisting of greenschist to amphibolite facies metamorphic rocks (schists, amphibolites) of Early- to Meso-Proterozoic age and Neoproterozoic rocks of the Sinian period (phyllites, slates, sandstones). Since the late 1950s, a number of giant

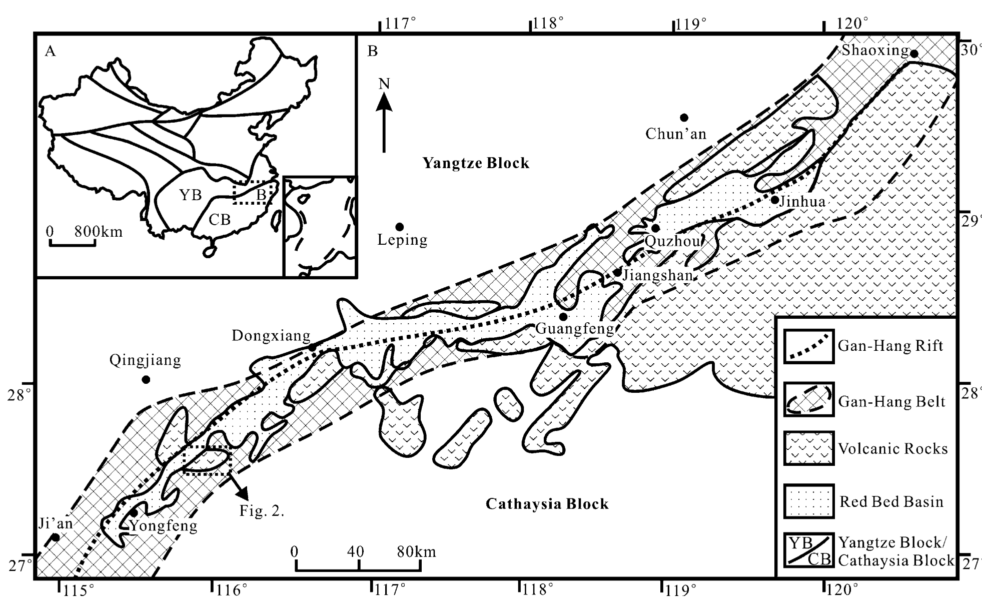

Fig. 1 Geological sketch map showing the Gan–Hang Belt in Southeast China. (Modified after Yu et al. 2006)

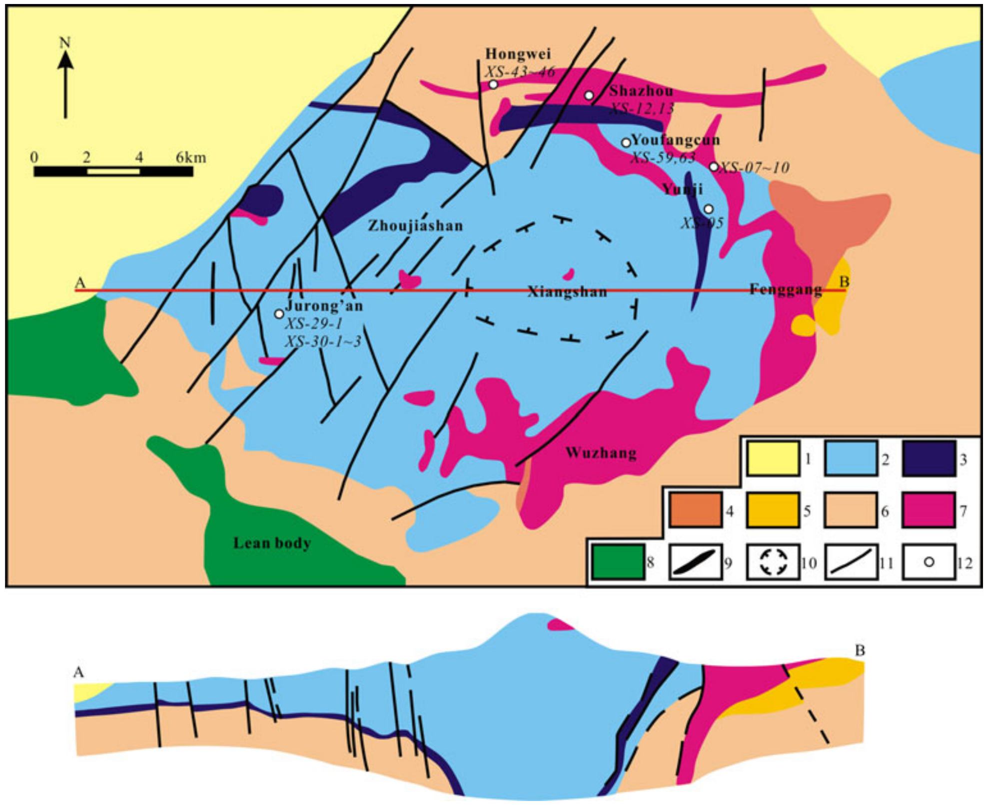

Fig. 2 Geological sketch map showing the volcanic-intrusive complex in the Xiangshan district (Modified after Fang et al. 1982; Fan et al. 2001a). *1*: glutenite; *2*: crystal tuffs and porphyritic lava; *3*: siltite and rhyodacite; *4*: gritstone and glutenite; *5*: gritstone; *6*: metamorphic rocks; *7*: granite porphyry; *8*: granite; *9*: lamprophyre dyke; *10*: lava neck (inferred); *11*: faults; *12*: sampling locations

uranium deposits have been explored and mined in this area. A series of Cretaceous-Tertiary red-bed basins were deposited in the Gan-Hang Belt (Fig. 1). The NE-trending basins are infilled with red clastic sedimentary rocks along with marls and evaporites (gypsum), which are locally interlayered with the volcanic rocks. The basins are mainly located to the NW of the volcanic-intrusive complex belt, and are thought to have been deposited in a back-arc extensional environment (Zhou and Li 2000).

The volcanic rocks from the Xiangshan include rhyolitic crystal tuffs, welded tuffs, rhyodacites (including rhyodacitic porphyry), acidic porphyritic lava, associated subvolcanic rocks such as monzogranite-porphyry and granite-porphyry, and late dykes such as quartz monzonitic porphyry and lamprophyre. The first volcanic cycle of the two previously distinguished magmatic cycles represents a fissure eruption and is composed mainly of rhyodacite that yielded a single-grain zircon U–Pb age of 158.1±0.2 Ma (Yu 2001) and rhyolitic welded tuff. Based on the geologic occurrence and petrologic characteristics, two types of rhyodacite were identified in the Xiangshan uranium ore field (Wu 1999). It was recognized that rhyodacite, which contains hematite bands, is of volcanic origin, but rhyodacitic porphyry without hematite bands belongs to a hypabyssal intrusive phase (Wu 1999). Field relations show that the rhyodacitic porphyry is intrusive and penetrates within rhyodacite, or as layers overlap the rhyodacite, and occurs as tongue-like bodies that interpenetrates clastoporphyritic extrusives (Wu 1999; Wu et al. 2003; Fan et al. 2005). The second volcanic cycle was a central vent eruption and was composed mainly of an intrusive facies and an extrusive facies of felsic porphyroclastics that constitute the main part of the Xiangshan volcanic-intrusive complex; that yielded a single-grain zircon U–Pb age of 140.3 Ma (Chen et al. 1999). After the effusion, the volcano collapsed, creating ring fractures. Finally, hypabyssal rocks, such as monzogranite-porphyry and granite-porphyry (with a single-grain zircon U–Pb age of 135.4 Ma, Chen et al. 1999), were intruded along the ring fractures, forming ring dykes (Fig. 2). Mafic magmatism also occurs in the Xiangshan area, including lamprophyre dykes (with a single-grain zircon U–Pb age of 125.1± 3.1 Ma, Fan et al. 2005) and quartz monzonitic porphyry dykes (with a singled-grain zircon U–Pb age of 129.5± 2.0 Ma, Fan et al. 2005). These subvolcanic rocks contain mafic microgranular enclaves (Fan et al. 2001b). More details on the petrography, mineralogy, lithogeochemistry, and isotope geochemistry of the Xiangshan volcanic-intrusive complex are provided in Jiang et al. (2005) and Yang et al. (2010), and references therein.

Petrology

The mineralogical and petrographic features of various types of rocks in the Xiangshan intrusive-volcanic complex are summarized in Table 1. In brief, the rhyodacite contains hematite bands and is purple in hand specimens with slight flow structures, whereas the rhyodacitic porphyry does not contain hematite bands and is gray-green in hand specimens. The porphyritic lavas make up the bulk of the Xiangshan volcanic-intrusive complex. The subvolcanic rocks are composed mainly of the monzogranite-porphyry and granite-porphyry. Quartz monzonitic porphyry crops out in the northern part of the volcanic-intrusive complex as small dykes cutting the basement metamorphic rocks.

Mafic microgranular enclaves (defined as “quenched enclaves” by Fan et al. 2001b and Jiang et al. 2005), are hosted by the subvolcanic rocks, which show ovoid bodies with the long axis ranging from several centimetres to 60 cm. Large enclaves contain back-veins and quenched margins. Within the enclaves, or at the boundary between the enclaves and the host rock, K-feldspar xenocrysts are rounded and show sieve-like resorption textures, filled by the enclave material. They are compositionally identical to K-feldspar in the host rocks (Fan et al. 2001b).

Sampling and analytical methods

Samples for this study have been collected from surface exposures, underground mines and open pits. All the samples were collected away from areas of uranium mineralization, and are thus largely unaltered. The sample locations are shown in Fig. 2.

CL imaging of zircon

The samples were processed through crushing, conventional magnetic and heavy liquid separation methods to extract zircons for U–Pb dating, and then zircon grains were handpicked under a binocular microscope for analysis. The zircon grains were mounted in epoxy, and then polished to section the crystals in half for analysis. Zircons were documented with transmitted and reflected light micrographs as well as cathodoluminescence (CL) images to reveal their internal structures. The CL images for LA–ICP–MS zircon U–Pb dating were taken using a MonoCL3+ detector (manufactured by Gatan, U.S.A.) attached to a scanning electron microscope at the State Key Laboratory of Continental Dynamics, Northwest University in Xi’an. While the CL images for SHRIMP zircon U–Pb dating were performed at the Scanning Electron Microscope Group of Beijing SHRIMP Center, Chinese Academy of Geological Sciences.

Zircon U–Pb dating

The LA–ICP–MS zircon U–Pb analyses for samples XS-05 and XS-59 were carried out at the State Key Laboratory for

Table 1 Lithology and mineralogy of the studied magmatic rock types from the Xiangshan volcanic-intrusive complex

Lithology	Color	Texture	Mineralogy
Rhyodacite	Purple	Porphyritic texture, felsitic or microcrystalline texture	Plagioclase, quartz, biotite with minor alkali feldspar, contains hematite bands
Rhyodacitic porphyry	Gray-green	Porphyritic texture, felsitic or microcrystalline texture	Plagioclase, quartz, biotite with minor alkali feldspar
Porphyritic lava	Light grey	Cataclastic texture, microcrystalline or fine-grained granitic texture for groundmass	Quartz, alkali feldspar, plagioclase, biotite
Subvolcanic rocks	Light grey	Porphyritic texture, fine-grained granitic texture for groundmass	Plagioclase, alkali feldspar, quartz, biotite and minor amphibole and pyroxene
Quartz monzonitic porphyry	Dark-gray	Porphyritic texture, fine-grained granitic texture for groundmass	Plagioclase, alkali feldspar, quartz, biotite
Mafic microgranular enclaves	Greyish black	Microcrystalline	Alkali feldspar, plagioclase, quartz, pyroxene, biotite and amphibole

Mineral Deposits Research using an Agilent 7500a ICP-MS equipped with a New Wave Research 213 nm laser ablation system at Nanjing University. The ablated material is transported in a He carrier gas through 3 mm i.d. PVC tubing and then combined with Ar in a 30 cm^3 mixing chamber prior to entering the ICP-MS for isotopic measurement. Mass discrimination of the mass spectrometer and residual elemental fractionation were corrected by calibration against a homogeneous zircon standard, GEMOC/GJ-1 (608 Ma). Samples are analyzed in 'runs' of ca. 15 analyses, which include ten to 12 unknowns, bracketed by two to four analyses of the standard. The unknowns include one analysis of a well-characterized zircon standard, Mud Tank (735 Ma), as an independent control on reproducibility and instrument stability, and a weighted mean age of 735±13 Ma (2σ, n=16) was obtained for Mud Tank zircon during our routine analyses. Analyses were carried out with a beam diameter of 30–40 μm, 5 Hz repetition rate, and energy of 10 to 20 J/cm^2. Data acquisition for each analysis took 100 s (40 s on background, 60 s on signal). Raw c ount rates for ^{206}Pb, ^{207}Pb, ^{208}Pb, ^{232}Th, and ^{238}U were collected for age determination. Detailed analytical procedures are similar to those described by Jackson et al. (2004). The raw ICP-MS data were exported in ASCII format and processed using GLITTER (Van Achterbergh et al. 2001). Common Pb contents were evaluated using the method described by Andersen (2002). The age calculations and plotting of Concordia diagrams were made using Isoplot v. 3.23 (Ludwig 2003).

The SHRIMP zircon U–Pb analyses for samples XS-29-1, XS-12, XS-30-2 and XS-63 were performed using the SHRIMP II ion microprobe at Curtin University of Technology, Australia, via a remote control system operated in the State Key Laboratory for Mineral Deposits Research, Nanjing University. A primary ion beam of 4.5 nA, 10 kV O^{-2} and 25 to 30 μm spot diameter were used. Mass was analyzed at a mass resolution of 5000 (1% peak height). The standard TEM zircons (417 Ma) of the Geological Survey of Australia were used to correct for inter-element fractionation. After every three unknown zircon measurements, the zircon standard (TEM) was measured to control the reproducibility and instrument stability, and a weighted mean age of 417± 3 Ma (2σ, n=13) was obtained for TEM zircon during our routine analyses. The ^{204}Pb based method of common Pb correction was applied. Details of the analytical processes, principles and parameters of the equipment have been previously published (Compston et al. 1984; Williams and Claesson 1987; Compston et al. 1992; Williams et al. 1996; Williams 1998; Song et al. 2002).

Zircon Lu–Hf isotopes

Zircon Hf isotope analyses were carried out using a Newwave UP213 laser-ablation microprobe, attached to a Neptune multi-collector ICP-MS at the Institute of Mineral Resources, Chinese Academy of Geological Sciences, Beijing. Instrumental conditions and data acquisition were comprehensively described by Wu et al. (2006) and Hou et al. (2007). A stationary spot was used for the present analyses, with a beam diameter of either 40 μm or 55 μm depending on the size of ablated zircon domains. Helium was used as the carrier gas to transport the ablated sample from the laser-ablation cell to the ICP-MS torch via an Ar gas mixing chamber. In order to correct the isobaric interferences of ^{176}Lu and ^{176}Yb on ^{176}Hf, ^{176}Lu/^{175}Lu and ^{176}Yb/^{173}Yb ratios (normalizing ratios of 0.02658 and 0.796218, respectively; Chu et al. 2002) were determined. The mass 176 isobaric interference correction functions can be expressed as:

$$^{176}\mathrm{Hf} = 176_{\mathrm{m}} - \left[^{175}\mathrm{Lu} \times \left(^{176}\mathrm{Lu}/^{175}\mathrm{Lu}\right)_{\mathrm{t}}\left(\mathrm{M}_{176}/\mathrm{M}_{175}\right)^{\beta(\mathrm{Lu})} + ^{173}\mathrm{Yb} \times \left(^{176}\mathrm{Yb}/^{173}\mathrm{Yb}\right)_{\mathrm{t}}\left(\mathrm{M}_{176}/\mathrm{M}_{173}\right)^{\beta(\mathrm{Yb})}\right]$$

$$\beta = \ln(\mathrm{R_m}/\mathrm{R_t})/\ln(\mathrm{M_A}/\mathrm{M_B}),$$

Where β is the mass bias coefficient, R_m is the measured ratio of the two isotopes and R_t is the accepted ratio of the two isotopes. Zircon GJ1 was used as the reference standard, with a weighted mean ^{176}Hf/^{177}Hf ratio of 0.282013±27 (2σ) during our routine analyses. It is not distinguishable from a weighted mean ^{176}Hf/^{177}Hf ratio of 0.282013±19 (2σ) (Elhlou et al. 2006) from in-situ analysis.

For the calculation of $\varepsilon_{Hf}(t)$ values, we have adopted a decay constant for ^{176}Lu of 1.867×10^{-11} $year^{-1}$ (Soderlund et al. 2004) and chondritic present-day values of ^{176}Lu/^{177}Hf (0.0336) and ^{176}Hf/^{177}Hf (0.282785) derived from Bouvier et al. (2008). Depleted mantle Hf model ages (T_{DM}) were calculated using the measured ^{176}Lu/^{177}Hf ratios of zircon, assuming that the depleted mantle reservoir has a $^{176}Hf/^{177}Hf=0.283250$ at present day, with a $^{176}Lu/^{177}Hf$ value of 0.0384 (Griffin et al. 2000). The mantle extraction model age (T_{DM}^{C}) for the source rocks of the magmas was calculated by projecting initial $^{176}Hf/^{177}Hf$ ratios of the zircon to the depleted mantle model growth line using a mean $^{176}Lu/^{177}Hf$ value (0.015) for average continental crust (Griffin et al. 2002).

Major and trace elements and Sr–Nd isotopes of whole-rocks

The samples for whole-rock chemical analysis were crushed to 200-mesh using an agate mill. Whole-rock major and trace elements, and Sr and Nd isotopic compositions were determined at the State Key Laboratory for Mineral Deposits Research, Nanjing University. The whole-rock major element compositions were determined by a Jobin Yvon 38S ICP-AES, whereas trace and rare earth elements (REEs) were measured by a Finnigan Element II HR-ICP-MS. About 50 mg of powered sample was dissolved in high-pressure Teflon bombs using a HF + HNO_3 mixture. Rh was used as an internal standard to monitor signal drift during counting. The analytical precision is better than 10% for most trace and rare earth elements. Detailed analytical procedures for trace and rare earth elements are described by Gao et al. (2003).

Sr and Nd isotopic compositions were measured using a Finnigan Triton TI TIMS following the methods of Pu et al. (2004, 2005). About 50 mg samples were dissolved in the same way as for trace element analyses. Complete separation of Sr was achieved by a combination of cation-exchange chromatography in H^+ form and pyridinium form with the DCTA complex. Nd was then separated from the REE fractions by cation-exchange resin using HIBA as eluent. After purification, the separated Sr was dissolved in 1 μL of 1N HCl and then loaded with TaF_5 solution onto W filaments for TIMS analysis. The separated Nd was dissolved in 1 μL of 1N HCl and then loaded with H_3PO_4 solution onto Re double-filaments. $^{87}Sr/^{86}Sr$ and $^{143}Nd/^{144}Nd$ ratios are reported normalized to $^{86}Sr/^{88}Sr$ ratio of 0.1194 and $^{146}Nd/^{144}Nd$ ratio of 0.7219, respectively. During the period of laboratory analysis, measurements of NIST SRM-987 Sr standard yielded $^{87}Sr/^{86}Sr$ ratio of 0.710252±16 (2σ, n=65), and the JNdi-1 Nd standard yielded $^{143}Nd/^{144}Nd$ ratio of 0.512121±16 (2σ, n=67). Total analytical blanks were 5×10^{-11} g for Sm and Nd and $(2\sim5)\times10^{-10}$ g for Rb and Sr. For the calculation of I_{Sr}, $\varepsilon_{Nd}(t)$ and Nd model ages, the following parameters were used: $\lambda_{Rb}=1.42\times10^{-11}$ year^{-1} (Steiger and Jäger 1977); $\lambda_{Sm}=6.54\times10^{-12}$ year^{-1} (Lugmair and Marti 1978); $(^{147}Sm/^{144}Nd)_{CHUR}=0.1967$ (Jacobsen and Wasserburg 1980); $(^{143}Nd/^{144}Nd)_{CHUR}=0.512638$ (Goldstein et al. 1984); $(^{143}Nd/^{144}Nd)_{DM}=0.513151$, $(^{147}Sm/^{144}Nd)_{DM}=0.2136$ (Liew and Hofmann 1988).

Results

Zircon U–Pb chronology

Porphyritic lava (samples XS-05, XS-29-1, XS-59)

Zircons in porphyritic lava are colorless or buff to transparent, euhedral to subhedral, elongate to stubby grains. Concentric zoning and a typical magmatic oscillatory zonation is common and no inherited cores were observed (see insets in Fig. 3a–c). The results are reported in Tables 2 and 3. All of the Th/U ratios of zircons for porphyritic lava vary between 0.25 and 1.83, mostly clustering around 0.4–0.6, consistent with a magmatic origin (Hoskin and Black 2000; Belousova et al. 2002). Thus, the zircons can represent the formation age of the rocks. The U–Pb concordia diagrams for porphyritic lavas are shown in Fig. 3a–c. The weighted mean $^{206}Pb/^{238}U$ age for samples XS-05 (Yunji), XS-29-1 (Jurong'an) and XS-59 (Youfangcun) are 136±1 Ma (2σ, MSWD=1.3), 132±1 Ma (2σ, MSWD=0.58) and 135±1 Ma (2σ, MSWD=1.5), respectively.

Granite porphyry (samples XS-12, XS-30-2)

Zircons are euhedral, up to 200 μm long, having length/width ratios of about 2:1. Most of them are relatively transparent and colorless. Euhedral concentric zoning is common in most crystals. No inherited zircon cores were observed. Th/U ratios mostly vary between 0.28 and 0.78. The results are listed in Table 3. The best estimate of the crystallization ages of samples XS-12 (Shazhou) and XS-30-2 (Jurong'an), based on the mean $^{206}Pb/^{238}U$ ratio, are 137±1 Ma (2σ, MSWD=0.81) and 137±1 Ma (2σ, MSWD=1.8) (Fig. 3d, e).

Quartz monzonitic porphyry (beschtauite, sample XS-63)

Zircons were mostly clear and euhedral with concentric zoning and length/width ratios of about 2:1. Rounded zircon cores are occasionally observed within a few idiomorphic grains. The results are listed in Table 3. One analysis of a zircon core (spot XS-63-5.2) is discordant, yielding a $^{207}Pb/^{206}Pb$ age of 1679 Ma. For 12 of 17 analyses, $^{206}Pb/^{238}U$ ratios are indistinguishable within analytical uncertainties, corresponding to a single age population with a weighted mean $^{206}Pb/^{238}U$ age of 136±1 Ma (2σ, MSWD=1.3) (Fig. 3f). This age is interpreted as the crystallization age of the quartz monzonitic porphyry (sample XS-63 from Youfangcun).

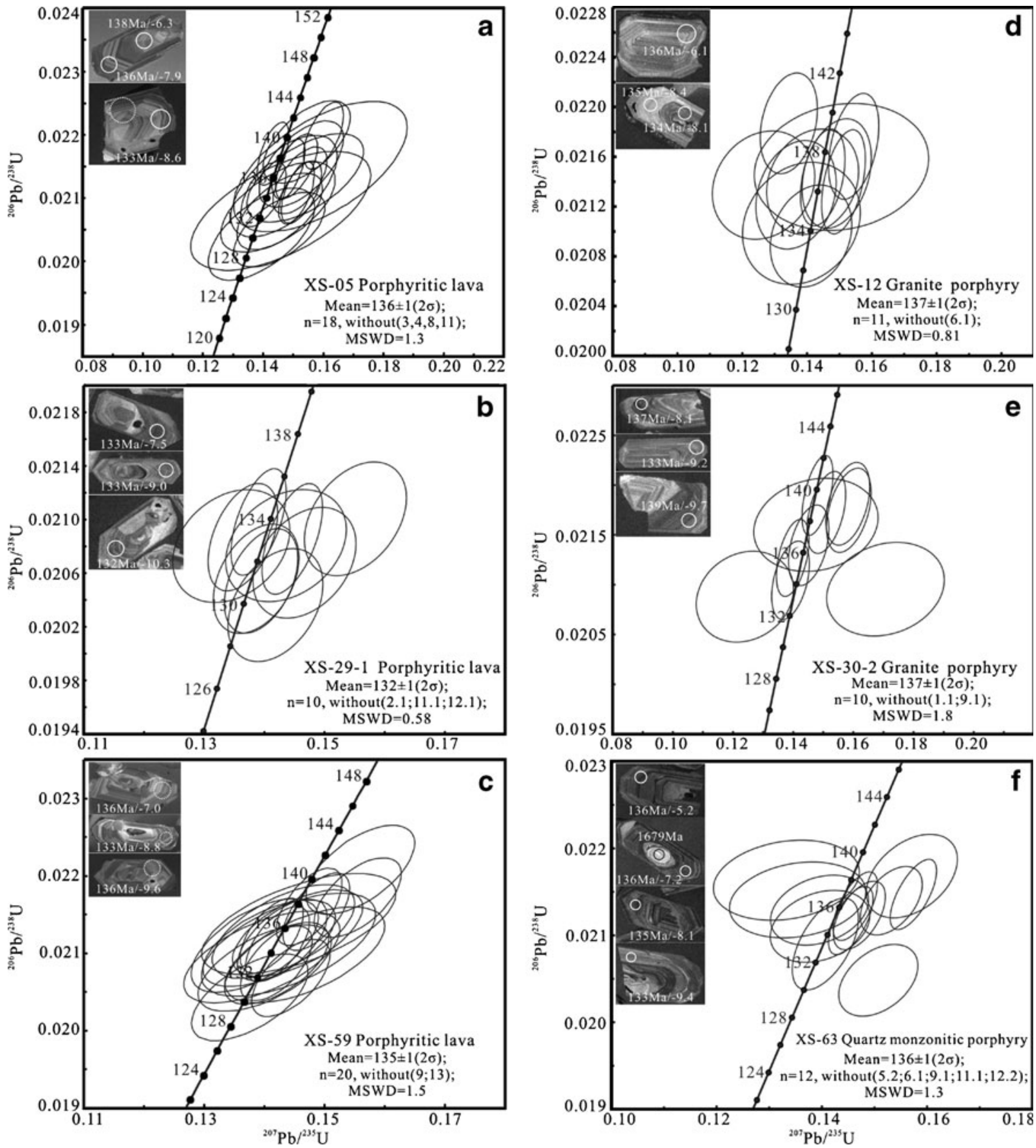

Fig. 3 Zircon U–Pb concordia diagram for porphyritic lava (**a**, **b**, **c**), granite porphyry (**d**, **e**) and quartz monzonitic porphyry (**f**) from Xiangshan volcanic-intrusive complex. The insets show typical CL images of zircons with ages and $\varepsilon_{Hf}(t)$ values. *Solid line circles* are the location of U–Pb analyses and *dotted line circles* are the location of Hf analysis spots in **a**, **c**. For **b**, **d**, **e**, **f**, *solid line circles* are the location of U–Pb analyses and Hf analysis spots

Geochemical and isotopic data

Major and trace elements

The Xiangshan volcanic-intrusive complex is peraluminous, with values of the alumina saturation index A/CNK >1.00 except for some subvolcanic rocks and a quartz monzonitic porphyry, which are metaluminous (A/CNK <1.00) (Fig. 4). The Xiangshan volcanic-intrusive complex has a wide range of chemical compositions, with SiO_2 of 62.52% to 76.94%, Al_2O_3 of 11.55% to 15.66%, MgO of 0.17% to 2.45%, Fe_{tot} of 1.10% to 5.63%, CaO of 0.56% to 4.00% (Table 4). The samples are relatively high in total alkali contents, with total K_2O + Na_2O ranging from 5.58% to 8.51%. The samples also have high K_2O contents, with all data plotting in the high-K calc-alkaline and shoshonite fields

Table 2 LA-ICPMS zircon U–Pb dating of porphyritic lava from Xiangshan volcanic-intrusive complex in SE China

Spot	U	Th	$^{232}Th/^{238}U$	$^{207}Pb/^{206}Pb$		$^{207}Pb/^{235}U$		$^{206}Pb/^{238}U$		$^{208}Pb/^{232}Th$		$^{207}Pb/^{206}Pb$		$^{207}Pb/^{235}U$		$^{206}Pb/^{238}U$		$^{208}Pb/^{232}Th$	
	ppm			Ratio	1σ	Ratio	1σ	Ratio	1σ	Ratio	1σ	Age/Ma	1σ	Age/Ma	1σ	Age/Ma	1σ	Age/Ma	1σ
XS-05 Porphyritic lava																			
XS-05-1	292	168	0.57	0.0508	0.0033	0.1455	0.0094	0.02079	0.00040	0.00576	0.00053	230	113	138	8	133	3	116	11
XS-05-2	234	171	0.73	0.0515	0.0036	0.1454	0.0100	0.02050	0.00039	0.00637	0.00052	262	123	138	9	131	2	128	10
XS-05-3	292	295	1.01	0.0609	0.0039	0.1685	0.0105	0.02006	0.00042	0.00645	0.00069	637	98	158	9	128	3	130	14
XS-05-4	386	318	0.82	0.0623	0.0028	0.1782	0.0080	0.02075	0.00038	0.00644	0.00055	684	64	167	7	132	2	130	11
XS-05-5	222	138	0.62	0.0504	0.0044	0.1449	0.0126	0.02086	0.00047	0.00660	0.00072	213	154	137	11	133	3	133	14
XS-05-6	278	154	0.55	0.0495	0.0042	0.1395	0.0117	0.02043	0.00048	0.00631	0.00073	173	145	133	10	130	3	127	15
XS-05-7	743	320	0.43	0.0508	0.0017	0.1506	0.0050	0.02150	0.00034	0.00569	0.00041	232	47	142	4	137	2	115	8
XS-05-8	800	356	0.44	0.0543	0.0025	0.1450	0.0064	0.01937	0.00035	0.00641	0.00071	384	67	137	6	124	2	129	14
XS-05-9	791	320	0.40	0.0524	0.0016	0.1523	0.0047	0.02109	0.00033	0.00632	0.00049	302	42	144	4	135	2	127	10
XS-05-10	1746	713	0.41	0.0504	0.0010	0.1490	0.0032	0.02146	0.00031	0.00583	0.00040	213	25	141	3	137	2	117	8
XS-05-11	381	357	0.94	0.0604	0.0038	0.1672	0.0102	0.02008	0.00044	0.00572	0.00066	618	93	157	9	128	3	115	13
XS-05-12	180	329	1.83	0.0524	0.0044	0.1540	0.0128	0.02132	0.00046	0.00715	0.00068	303	149	145	11	136	3	144	14
XS-05-13	1752	673	0.38	0.0521	0.0012	0.1515	0.0036	0.02109	0.00032	0.00657	0.00063	291	28	143	3	135	2	132	13
XS-05-14	382	273	0.72	0.0503	0.0041	0.1470	0.0117	0.02119	0.00053	0.00633	0.00071	211	134	139	10	135	3	128	14
XS-05-15	660	314	0.48	0.0483	0.0017	0.1401	0.0050	0.02106	0.00034	0.00635	0.00052	113	53	133	4	134	2	128	10
XS-05-16	513	239	0.47	0.0519	0.0020	0.1523	0.0059	0.02128	0.00035	0.00715	0.00070	281	58	144	5	136	2	144	14
XS-05-17	1229	504	0.41	0.0479	0.0011	0.1433	0.0035	0.02170	0.00033	0.00577	0.00041	95	30	136	3	138	2	116	8
XS-05-18	139	100	0.72	0.0509	0.0070	0.1459	0.0197	0.02080	0.00062	0.00767	0.00124	237	246	138	17	133	4	154	25
XS-05-19	967	712	0.74	0.0528	0.0014	0.1601	0.0044	0.02199	0.00035	0.00663	0.00051	321	34	151	4	140	2	134	10
XS-05-20	395	195	0.49	0.0514	0.0032	0.1527	0.0093	0.02154	0.00045	0.00770	0.00090	261	101	144	8	137	3	155	18
XS-05-21	268	174	0.65	0.0512	0.0032	0.1545	0.0096	0.02189	0.00043	0.00719	0.00065	250	106	146	8	140	3	145	13
XS-05-22	206	137	0.67	0.0537	0.0066	0.1590	0.0191	0.02150	0.00068	0.00757	0.00170	356	212	150	17	137	4	152	34
XS-59 Porphyritic lava																			
XS-59-1	150	70	0.47	0.0495	0.0037	0.1457	0.0107	0.02138	0.00043	0.00727	0.00074	169	128	138	9	136	3	146	15
XS-59-2	491	217	0.44	0.0519	0.0016	0.1555	0.0048	0.02172	0.00034	0.00872	0.00059	282	42	147	4	139	2	175	12
XS-59-3	741	295	0.40	0.0501	0.0012	0.1486	0.0037	0.02154	0.00033	0.00646	0.00033	197	30	141	3	137	2	130	7
XS-59-4	208	132	0.63	0.0496	0.0024	0.1455	0.0071	0.02126	0.00037	0.00714	0.00042	178	81	138	6	136	2	144	8
XS-59-5	209	104	0.50	0.0483	0.0025	0.1408	0.0073	0.02113	0.00037	0.00705	0.00047	115	85	134	6	135	2	142	9
XS-59-6	292	208	0.71	0.0494	0.0020	0.1420	0.0057	0.02087	0.00035	0.00676	0.00040	164	63	135	5	133	2	136	8
XS-59-7	858	211	0.25	0.0495	0.0011	0.1474	0.0036	0.02160	0.00033	0.00694	0.00043	172	30	140	3	138	2	140	9
XS-59-8	1035	477	0.46	0.0488	0.0011	0.1422	0.0035	0.02112	0.00032	0.00673	0.00041	139	31	135	3	135	2	136	8
XS-59-9	360	210	0.58	0.0512	0.0020	0.1559	0.0060	0.02208	0.00038	0.00710	0.00047	251	56	147	5	141	2	143	9

XS-59-10	575	271	0.47	0.0494	0.0013	0.1420	0.0040	0.02087	0.00032	0.00658	0.00039	164	37	135	4	133	2	133	8
XS-59-11	288	259	0.90	0.0507	0.0031	0.1467	0.0088	0.02098	0.00041	0.00654	0.00060	228	101	139	8	134	3	132	12
XS-59-12	287	184	0.64	0.0495	0.0034	0.1440	0.0096	0.02111	0.00044	0.00863	0.00093	170	112	137	8	135	3	174	19
XS-59-13	470	371	0.79	0.0538	0.0020	0.1239	0.0046	0.01671	0.00028	0.00381	0.00022	362	54	119	4	107	2	77	4
XS-59-14	1242	546	0.44	0.0490	0.0017	0.1430	0.0049	0.02117	0.00035	0.00696	0.00080	147	50	136	4	135	2	140	16
XS-59-15	307	347	1.13	0.0488	0.0027	0.1432	0.0078	0.02128	0.00040	0.00686	0.00058	138	90	136	7	136	3	138	12
XS-59-16	310	262	0.85	0.0488	0.0026	0.1400	0.0073	0.02081	0.00037	0.00588	0.00046	139	86	133	7	133	2	118	9
XS-59-17	421	251	0.60	0.0476	0.0024	0.1384	0.0070	0.02110	0.00040	0.00624	0.00043	78	77	132	6	135	3	126	9
XS-59-18	756	347	0.46	0.0507	0.0015	0.1444	0.0043	0.02068	0.00033	0.00594	0.00035	225	40	137	4	132	2	120	7
XS-59-19	469	237	0.51	0.0489	0.0023	0.1376	0.0064	0.02043	0.00037	0.00562	0.00048	141	74	131	6	130	2	113	10
XS-59-20	944	420	0.44	0.0482	0.0011	0.1412	0.0035	0.02123	0.00032	0.00631	0.00036	111	31	134	3	135	2	127	7
XS-59-21	225	147	0.65	0.0483	0.0030	0.1396	0.0086	0.02095	0.00039	0.00675	0.00053	115	103	133	8	134	2	136	11

in a K_2O vs SiO_2 classification diagram, except for quartz monzonitic porphyry that is medium-K calc-alkaline (Fig. 5g). On binary major and trace element vs SiO_2 variation diagrams (Fig. 5a–f), samples from the volcanic-intrusive complex show a general decrease in Al_2O_3, TiO_2, Fe_{tot} ($FeO + Fe_2O_3$), MgO, CaO, and P_2O_5, whereas K_2O (Fig. 5g) and Na_2O (not shown) do not correlate with SiO_2.

Chondrite-normalized REE patterns of the Xiangshan volcanic-intrusive complex invariably show light REE (LREE) enrichment and negative Eu anomalies (Fig. 6a). LREE are enriched relative to HREE in all rocks (LREE/HREE=3.98 to 17.85). Differences between samples are most pronounced in the LREE abundances (La_N=58 to 308), REE pattern slopes (La_N/Yb_N=3.47 to 29.33) and degree of the Eu anomaly (Eu/Eu*=0.18 to 0.82) (Table 4). In the primitive mantle-normalized variation diagrams, all the Xiangshan volcanic-intrusive rocks show enrichment in Rb and Th (U) and characteristic depletion in Ba, Nb (Ta), Sr, P and Ti (Table 4) (Fig. 6b). The samples are rich in high field strength elements and Ga with high Ga/Al ratios. Samples from enclave centers which show the least chemical modification and therefore can be considered as representative compositions of the mafic microgranular enclave magma show the following geochemical characteristics (Jiang et al. 2005): intermediate SiO_2 contents, high MgO and low TiO_2 contents, high Mg-numbers and high concentrations of Sc, Ni, Co and V; enrichment in alkalis, high K_2O contents with high K_2O/Na_2O ratios, high light REE and large ion lithophile element contents, low initial $\varepsilon_{Nd}(T)$ values (−4.2) and high initial $^{87}Sr/^{86}Sr$ ratios (0.708147).

Sr–Nd isotopic compositions

Eighteen samples from the Xiangshan volcanic-intrusive complex show a wide range of calculated $^{87}Rb/^{86}Sr$ (1.26 to 20.23) and measured $^{87}Sr/^{86}Sr$ (0.712489 to 0.750231) ratios due to significant fractionation and variable chemical compositions, while their age-corrected initial $^{87}Sr/^{86}Sr$ (I_{Sr}) ratios cluster between 0.708516 and 0.715057 (Table 5). The Xiangshan volcanic-intrusive complex also displays variable calculated $^{147}Sm/^{144}Nd$ ratios ranging from 0.09 to 0.17, and measured $^{143}Nd/^{144}Nd$ ratios between 0.512098 and 0.512268. Calculated initial $\varepsilon_{Nd}(T)$ values range from −6.9 to −8.7 and the T_{DM}^C model ages are mostly between 1.49 and 1.64 Ga (Table 5), except for the quartz monzonitic porphyry sample which has a higher $\varepsilon_{Nd}(T)$ value of −5.7 and a younger T_{DM}^C model age of 1.40 Ga. The mafic microgranular enclaves center has a relatively high $\varepsilon_{Nd}(T)$ value (−4.2) with the T_{DM}^C model age of 1.27 Ga, and a low initial $^{87}Sr/^{86}Sr$ value (0.708058).

Table 3 SHRIMP zircon U–Pb dating of porphyritic lava, granite porphyry and quartz monzonitic porphyry from Xiangshan volcanic-intrusive complex in SE China

Spot	$^{206}Pb_c$	U	Th	$^{232}Th/^{238}U$	$^{206}Pb^*$	$^{207}Pb^*/^{206}Pb^*$		$^{207}Pb^*/^{235}U$		$^{206}Pb^*/^{238}U$		$^{207}Pb/^{206}Pb$		$^{208}Pb/^{232}Th$		$^{206}Pb/^{238}U$	
	(%)	ppm			ppm	Ratio	1σ	Ratio	1σ	Ratio	1σ	Age/Ma	1σ	Age/Ma	1σ	Age/Ma	1σ
XS-29-1 Porphyritic lava																	
XS29-1-1.1	0.21	577	209	0.37	10.40	0.0474	0.0012	0.1364	0.0038	0.02087	0.00027	70	59	129	4	133	2
XS29-1-2.1	0.25	395	173	0.45	7.18	0.0603	0.0042	0.1750	0.0124	0.02109	0.00027	616	150	152	8	135	2
XS29-1-3.1	0.55	394	164	0.43	7.08	0.0469	0.0022	0.1345	0.0065	0.02080	0.00027	44	110	126	6	133	2
XS29-1-4.1	–	649	216	0.34	11.70	0.0481	0.0009	0.1390	0.0031	0.02098	0.00027	102	42	136	3	134	2
XS29-1-5.1	0.00	553	194	0.36	9.91	0.0503	0.0010	0.1446	0.0033	0.02086	0.00027	209	44	137	3	133	2
XS29-1-6.1	–	377	171	0.47	6.78	0.0536	0.0018	0.1551	0.0056	0.02101	0.00027	353	76	140	5	134	2
XS29-1-7.1	0.23	440	180	0.42	7.88	0.0501	0.0022	0.1436	0.0066	0.02081	0.00027	198	100	132	6	133	2
XS29-1-8.1	–	438	253	0.60	7.76	0.0514	0.0019	0.1467	0.0057	0.02068	0.00027	261	83	134	4	132	2
XS29-1-9.1	0.01	901	268	0.31	15.90	0.0492	0.0013	0.1395	0.0040	0.02054	0.00027	159	61	130	3	131	2
XS29-1-10.1	–	574	164	0.29	10.10	0.0489	0.0015	0.1386	0.0047	0.02056	0.00027	144	73	134	5	131	2
XS29-1-11.1	–	414	165	0.41	6.96	0.0541	0.0030	0.1469	0.0085	0.01970	0.00028	374	130	131	7	126	2
XS29-1-12.1	0.20	558	203	0.38	9.41	0.0477	0.0015	0.1287	0.0045	0.01958	0.00025	83	76	120	4	125	2
XS29-1-13.1	–	425	185	0.45	7.43	0.0505	0.0017	0.1418	0.0052	0.02036	0.00029	219	79	138	4	130	2
XS-12 Granite porphyry																	
XS12-1.1	0.90	255	146	0.59	4.71	0.0465	0.0027	0.1366	0.0082	0.02129	0.00030	25	140	130	7	136	2
XS12-2.1	0.60	565	196	0.36	10.70	0.0446	0.0019	0.1344	0.0058	0.02187	0.00026	-79	100	126	6	140	2
XS12-3.1	1.20	314	134	0.44	5.84	0.0430	0.0035	0.1270	0.0104	0.02137	0.00028	-170	200	121	9	137	2
XS12-4.1	0.34	681	237	0.36	12.60	0.0490	0.0014	0.1448	0.0045	0.02143	0.00026	148	68	136	5	137	2
XS12-5.1	0.41	181	81	0.46	3.35	0.0508	0.0061	0.1510	0.0181	0.02152	0.00034	230	270	134	14	137	2
XS12-6.1	–	97	44	0.47	1.84	0.0658	0.0029	0.2021	0.0095	0.02229	0.00036	799	92	178	8	139	2
XS12-7.1	0.10	235	123	0.54	4.33	0.0504	0.0023	0.1492	0.0070	0.02147	0.00030	213	110	142	5	137	2
XS12-8.1	0.18	295	204	0.71	5.51	0.0516	0.0016	0.1544	0.0051	0.02168	0.00028	269	70	136	4	138	2
XS12-9.1	0.20	307	142	0.48	5.66	0.0513	0.0013	0.1512	0.0044	0.02140	0.00028	252	61	139	4	136	2
XS12-10.1	0.48	384	290	0.78	7.09	0.0480	0.0031	0.1417	0.0094	0.02140	0.00028	101	150	128	5	137	2
XS12-11.1	0.89	143	70	0.51	2.61	0.0476	0.0040	0.1380	0.0120	0.02107	0.00032	79	200	137	9	135	2
XS12-11.2	0.43	397	177	0.46	7.18	0.0489	0.0028	0.1412	0.0083	0.02096	0.00027	141	130	125	7	134	2
XS-30-2 Granite porphyry																	
XS-30-2-01	0.55	704	228	0.33	12.7	0.0461	0.0020	0.1325	0.0060	0.02083	0.00027	5	100	118	7	133	2
XS-30-2-02	–	894	243	0.28	16.7	0.0526	0.0015	0.1581	0.0047	0.02181	0.00028	311	63	152	7	139	2
XS-30-2-03	0.15	945	254	0.28	17.4	0.0492	0.0014	0.1452	0.0044	0.02140	0.00026	158	65	128	5	137	2
XS-30-2-04	0.42	386	148	0.40	7.2	0.0495	0.0045	0.1480	0.0136	0.02160	0.00030	174	210	135	13	138	2
XS-30-2-05	0.05	1099	323	0.30	20.7	0.0490	0.0009	0.1481	0.0034	0.02190	0.00026	150	46	138	4	140	2
XS-30-2-06	0.10	685	262	0.40	12.8	0.0504	0.0013	0.1510	0.0042	0.02173	0.00028	214	59	132	4	139	2

XS-30-2-07	–	660	218	0.34	12.3	0.0528	0.0015	0.1585	0.0049	0.02175	0.00028	322	64	147	5	139	2
XS-30-2-09	0.03	778	223	0.30	13.6	0.0488	0.0009	0.1366	0.0031	0.02031	0.00024	137	44	127	4	130	2
XS-30-2-10	0.18	1177	395	0.35	21.3	0.0479	0.0013	0.1391	0.0042	0.02104	0.00025	96	64	128	4	134	2
XS-30-2-11	–	255	110	0.44	4.6	0.0591	0.0044	0.1710	0.0130	0.02095	0.00031	570	160	161	11	134	2
XS-30-2-12	0.24	1414	541	0.40	25.9	0.0477	0.0011	0.1398	0.0036	0.02127	0.00026	84	54	125	4	136	2
XS-30-2-13	1.02	279	127	0.47	5.1	0.0430	0.0037	0.1240	0.0107	0.02088	0.00029	-165	210	120	9	133	2
XS-63 Quartz monzonitic porphyry																	
XS63-1.1	–	631	129	0.21	11.10	0.0534	0.0016	0.1507	0.0050	0.02048	0.00027	345	68	149	8	131	2
XS63-2.1	0.22	1008	371	0.38	18.10	0.0488	0.0012	0.1407	0.0042	0.02090	0.00036	139	57	131	4	133	2
XS63-3.1	0.36	936	307	0.34	17.20	0.0475	0.0020	0.1396	0.0061	0.02129	0.00026	77	100	128	7	136	2
XS63-4.1	0.44	757	127	0.17	13.80	0.0480	0.0021	0.1397	0.0063	0.02110	0.00027	99	100	120	13	135	2
XS63-5.1	–	1000	336	0.35	18.30	0.0498	0.0007	0.1464	0.0028	0.02134	0.00026	184	34	138	3	136	2
XS63-5.2	0.08	631	146	0.24	38.50	0.1030	0.0014	1.0070	0.0191	0.07094	0.00092	1679	26	218	7	442	6
XS63-6.1	1.28	259	133	0.53	4.58	0.0463	0.0043	0.1300	0.0121	0.02035	0.00031	13	220	125	9	130	2
XS63-7.1	0.00	970	329	0.35	17.70	0.0503	0.0010	0.1471	0.0032	0.02123	0.00025	208	43	134	3	135	2
XS63-8.1	–	1160	406	0.36	21.30	0.0519	0.0011	0.1532	0.0038	0.02140	0.00026	282	51	139	4	137	2
XS63-9.1	0.41	277	28	0.10	5.76	0.0517	0.0022	0.1722	0.0077	0.02415	0.00034	273	98	171	23	154	2
XS63-10.1	–	927	317	0.35	16.90	0.0498	0.0007	0.1455	0.0028	0.02117	0.00025	188	34	138	3	135	2
XS63-11.1	0.20	2531	1137	0.46	49.30	0.0503	0.0007	0.1570	0.0028	0.02263	0.00027	209	33	148	3	144	2
XS63-11.2	1.58	307	229	0.77	5.81	0.0447	0.0030	0.1333	0.0092	0.02163	0.00030	-73	160	127	5	138	2
XS63-11.3	–	216	315	1.51	4.02	0.0526	0.0017	0.1571	0.0057	0.02168	0.00033	310	76	135	3	138	2
XS63-12.1	–	930	338	0.38	17.10	0.0532	0.0007	0.1574	0.0028	0.02147	0.00026	336	31	142	3	137	2
XS63-12.2	1.31	190	65	0.35	3.37	0.0448	0.0036	0.1260	0.0102	0.02035	0.00031	-68	190	117	12	130	2
XS63-13.1	1.02	405	168	0.43	7.52	0.0459	0.0028	0.1354	0.0085	0.02141	0.00028	-9	150	126	8	137	2

Pb_c and Pb^* indicate the common and radiogenic portions, respectively

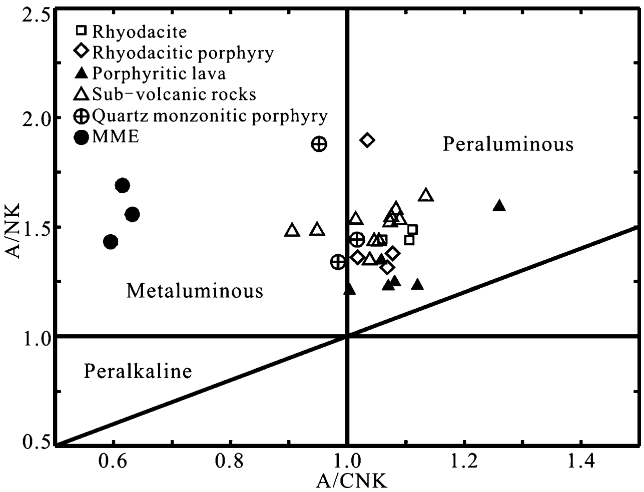

Fig. 4 A/NK vs A/CNK diagram (Maniar and Piccoli 1989) showing the peraluminous character of volcanic-intrusive complex and the metaluminous character of mafic microgranular enclaves from Xiangshan. A = Al_2O_3, C = CaO, N = Na_2O, K = K_2O (all in molar proportion)

Zircon Hf isotopic compositions

Twenty-one spot analyses of Hf isotopes were obtained for rhyodacite (Sample XS-30-1, Yang et al. 2010), yielding ε_{Hf}(T) values between −5.7 and −8.5 (Fig. 7a), corresponding to T_{DM}^{C} model ages between 1,550 Ma and 1,720 Ma (Fig. 7f). Both the ε_{Hf}(T) values and T_{DM}^{C} model ages show nearly unimodal distributions, with an average of ε_{Hf}(T)=−7.0 and T_{DM}^{C}=1,630 Ma.

Eighteen spot analyses were obtained for a rhyodacitic porphyry (Sample XS-30-3, Yang et al. 2010), yielding ε_{Hf}(T) values between −6.9 and −10.1 (Fig. 7b), corresponding to T_{DM}^{C} Hf model ages between 1,621 Ma and 1,823 Ma (Fig. 7g). Both the ε_{Hf}(T) values and T_{DM}^{C} Hf model ages show nearly unimodal distributions, with an average of ε_{Hf}(T) of −8.5 and T_{DM}^{C} Hf model age of 1,721 Ma.

Sixty-one spots of in situ Hf isotope analysis have been determined on zircon from porphyritic lava (sample XS-05, XS-29-1 and XS-59) (Table 6). Zircons in porphyritic lava are characterized by clearly negative initial ε_{Hf} values, ranging from −6.3 to −10.3 with a weighted mean of −8.3 (Fig. 7c), and corresponding to T_{DM}^{C} Hf model ages between 1,585 Ma and 1,832 Ma with an average of T_{DM}^{C} Hf model age of 1,706 Ma (Fig. 7h).

Thirty-four spots were analysed on zircon from subvolcanic-rocks (sample XS-12 and XS-30-2) (Table 6). All domains show negative ε_{Hf}(T) values between −6.1 and −9.9 with a average of −8.6 (Fig. 7d). Correspondingly, their Hf model ages are 1571 to 1813 Ma, with an average of 1731 Ma (Fig. 7i).

Twenty-one spots were analysed on zircon from quartz monzonitic porphyry (Sample XS-63) (Table 6). Uniformly negative ε_{Hf}(T) values scatter between −5.2 and −10.2, with an average of −7.7 (Fig. 7e). Correspondingly, their Hf model ages are 1514 to 1832 Ma with an average of 1672 Ma (Fig. 7j).

A summary of Hf isotopic data for all zircons from the Xiangshan volcanic-intrusive complex is presented in Table 7. Overall, Hf isotopic data of the zircons are all negative and show nearly unimodal distributions, and T_{DM}^{C} of late Paleo-Mesoproterozoic ages.

Discussion

Timing of the Xiangshan volcanic-intrusive complex

Previously published geochronological data suggest that the formation of the Xiangshan volcanic-intrusive complex corresponds to two cycles of volcanic-intrusive activity mainly in the Late Jurassic (158–135 Ma) (Jiang et al. 2005), which lasted for more than 20 million years.

In this study, the high spatial resolution zircon U-Pb dating results demonstrate that emplacement of the various igneous units at Xiangshan took place within a rather short time span (ca. 2 Ma). Our new data indicate that the Xiangshan volcanic-intrusive complex was formed during a Cretaceous magmatic event in SE China that was generated in response to the peak of an extensional tectonic regime (Li 2000). The Xiangshan complex comprises a series of felsic volcanic and intrusive rocks that overlie the Mesoproterozoic basement. The stratigraphically oldest rhyodacite yielded a U–Pb zircon age of 135±1 Ma. The overlying rhyodacitic porphyry was dated at 135±1 Ma (Yang et al. 2010). Our new ages for three porphyritic lava samples from Yunji (Sample XS-05), Jurong'an (Sample XS-29-1), Youfangcun (Sample XS-59) area are 136±1 Ma, 132±1 Ma and 135±1 Ma, respectively. The felsic magmas at Xiangshan is composed of sub-volcanic rocks (granite porphyry). This unit yielded U–Pb zircon ages of 137±1 (Shazhou, Sample XS-12) and 137±1 Ma (Jurong'an, Sample XS-30-2), respectively. The final stage of magmatism at Xiangshan involved emplacement of quartz monzonitic porphyry dykes and lamprophyric dykes. The quartz monzonitic porphyry yielded a U–Pb zircon age of 136±1 Ma (Youfangcun, Sample XS-63). All these ages are identical within analytical errors.

The precise zircon U–Pb dating of magmatic events at Xiangshan demonstrates that the volcanic-intrusive activity is ephemeral. Field relations indicate that the intrusive

Table 4 Major (wt.%) and trace element (ppm) compositions of the Xiangshan volcanic-intrusive complex and mafic microgranular enclave in SE China

	Rhyodacite			Rhyodacitic porphyry				Porphyritic lava					
	XS-30-1	X9-18[a]	X9-19[a]	X9-20[a]	X9-25[a]	X9-26[a]	X9-27[a]	XS-29-1	XS-59	X9-21[a]	X9-22[a]	X9-24[a]	X9-28[a]
SiO_2	69.55	68.48	68.59	67.80	68.64	69.00	67.47	74.41	76.94	76.79	76.06	76.05	74.97
TiO_2	0.43	0.39	0.44	0.37	0.40	0.38	0.35	0.20	0.13	0.08	0.1	0.09	0.08
Al_2O_3	13.73	14.82	14.78	14.35	14.56	14.23	15.10	12.89	12.52	11.92	12.35	12.48	11.55
Fe_2O_3	3.53	3.08	3.28	1.65	1.80	2.37	1.77	0.16	0.16	0.47	0.6	0.41	1.48
FeO	1.16	0.37	0.42	1.85	1.54	1.21	1.40	2.01	1.62	0.63	0.8	0.98	1.21
MnO	0.11	0.07	0.07	0.11	0.07	0.07	0.08	0.10	0.09	0.04	0.06	0.04	0.05
MgO	0.42	0.87	0.58	0.93	0.87	0.76	0.87	0.28	0.17	0.27	0.27	0.21	0.32
CaO	1.89	1.71	1.85	1.96	1.41	1.59	1.77	1.44	1.14	0.79	0.84	0.56	1.07
Na_2O	3.74	2.92	2.77	3.17	3.58	3.00	3.70	2.65	2.11	2.88	2.88	2.82	2.62
K_2O	3.11	5.07	4.97	4.92	4.78	4.97	4.92	4.81	4.06	4.59	4.77	5.07	4.85
P_2O_5	0.17	0.18	0.19	0.18	0.17	0.16	0.19	0.08	0.07	0.03	0.04	0.06	0.06
LOI	2.28	2.17	1.35	2.25	1.76	1.87	1.69	0.82	0.70	0.95	0.53	0.71	1.11
Total	100.12	100.13	99.30	99.54	99.58	99.61	99.31	99.85	99.71	99.44	99.3	99.48	99.37
A.R.	2.56	2.87	2.74	2.97	3.20	3.03	3.09	3.17	2.65	3.85	3.76	4.06	3.90
ACNK	1.06	1.11	1.11	1.02	1.07	1.08	1.03	1.06	1.26	1.07	1.08	1.12	1.00
ANK	1.44	1.44	1.49	1.36	1.32	1.38	1.32	1.35	1.59	1.23	1.25	1.23	1.21
Ga	20.4	25.0	25.0	26.0	22.0	23.0	–	19.4	17.9	19.0	19.0	21.0	19.0
Rb	227	296	279	293	273	296	–	254	290	315	276	240	268
Ba	190	213	244	140	174	180	–	116	71.8	35.0	70.0	162	59.0
Th	28.1	29.0	29.0	30.0	27.0	29.0	–	24.1	26.9	27.0	27.0	27.0	28.0
U	249	221	258	223	236	187	–	231	140	85.0	146	239	103
Nb	19.3	22.0	22.0	23.0	22.0	22.0	–	16.5	15.2	18.0	20.0	20.0	15.0
Ta	352	530	501	428	554	539	–	217	109	50.0	84.0	372	105
Sr	6.09	5.90	7.20	6.40	6.70	5.90	–	6.16	4.39	3.80	5.10	6.60	4.10
Zr	2.14	2.19	2.34	2.34	2.39	2.44	–	1.61	1.81	3.08	2.52	1.65	2.10
Hf	22.5	24.0	25.0	24.0	23.0	24.0	–	23.5	22.7	22.0	24.0	23.0	27.0
Y	7.63	6.20	5.80	11.60	7.90	8.30	–	6.08	7.76	10.5	11.4	7.20	14.8
La	48.5	54.0	53.0	51.0	51.0	49.0	–	52.9	30.8	18.0	31.0	65.0	33.0
Ce	97.6	128	115	123	115	114	–	108	74.5	35.0	71.0	160	79.0
Pr	10.7	15.2	15.0	14.8	14.9	13.7	–	11.7	8.02	5.70	9.90	17.7	10.5
Nd	35.4	53.0	51.0	50.0	51.0	46.0	–	37.9	26.3	21.0	35.0	59.0	36.0
Sm	7.30	8.40	8.20	7.70	8.10	7.90	–	7.31	5.83	4.60	6.50	8.50	6.70
Eu	0.91	1.48	1.30	1.20	1.18	1.25	–	0.73	0.50	0.27	0.47	1.17	0.53
Gd	6.26	8.20	8.40	8.00	8.10	7.90	–	5.78	5.09	4.70	5.80	8.50	6.50
Tb	0.87	1.19	1.15	1.13	1.13	1.19	–	0.75	0.74	0.88	0.93	1.10	0.95
Dy	5.60	6.40	6.50	6.40	6.40	6.80	–	4.74	5.04	5.80	5.50	5.70	5.60
Ho	1.14	1.29	1.32	1.35	1.35	1.41	–	0.91	1.05	1.24	1.21	1.17	1.15
Er	3.25	3.70	3.70	4.10	3.90	4.10	–	2.57	3.06	3.90	3.70	3.30	3.40
Tm	0.50	0.56	0.56	0.58	0.56	0.59	–	0.41	0.47	0.59	0.53	0.47	0.50

Table 4 (continued)

		Rhyodacite					Rhyodacitic porphyry				Porphyritic lava					
		XS-30-1		X9-18[a]		X9-19[a]	X9-20[a]	X9-25[a]	X9-26[a]	X9-27[a]	XS-29-1	XS-59	X9-21[a]	X9-22[a]	X9-24[a]	X9-28[a]
Yb		2.80		3.30		3.30	3.40	3.30	3.40	–	2.34	2.83	3.50	3.10	2.70	3.00
Lu		0.44		0.57		0.56	0.59	0.58	0.59	–	0.37	0.43	0.63	0.55	0.47	0.52
ΣREE		221.3		285.3		269.0	273.3	266.5	257.8	–	236.2	164.6	105.8	175.2	334.8	187.4
LREE/HREE		9.61		10.32		9.55	9.69	9.53	8.92	–	12.21	7.79	3.98	7.22	13.30	7.67
$(La/Yb)_N$		11.66		11.03		10.83	10.11	10.42	9.72	–	15.23	7.35	3.47	6.74	16.23	7.42
$(La/Sm)_N$		4.18		4.04		4.07	4.17	3.96	3.90	–	4.55	3.33	2.46	3.00	4.81	3.10
Eu/Eu*		0.40		0.54		0.47	0.46	0.44	0.48	–	0.33	0.27	0.18	0.23	0.42	0.24
Granite porphyry											Quartz monzonitic porphyry			Mafic microgranular enclave		
XS-07	XS-08	XS-09	XS-10	XS-12	XS-13	XS-43	X9-12[a]	X9-15[a]	SB-1[a]	SB-2[a]	XS-63	89-30[b]	C-25[b]	SB-4[c]	SB-5[c]	99-5[c]
71.52	69.61	70.52	69.76	69.53	71.22	70.23	65.35	67.61	68.83	69.07	63.35	62.52	64.24	53.76	54.3	54.66
0.40	0.36	0.36	0.36	0.44	0.34	0.32	0.42	0.38	0.32	0.34	0.59	0.80	0.84	0.47	0.5	0.48
14.66	14.28	14.22	14.19	15.00	13.96	14.72	15.63	15	13.53	13.3	14.03	15.66	14.82	11.69	11.75	12.09
0.92	0.63	0.74	0.84	0.60	0.61	0.05	0.88	0.93	1.29	1.27	0.94	0.90	0.75	2.27	2.06	2.21
1.98	2.07	1.96	1.83	2.54	1.90	2.20	3.13	2.12	1.66	2.45	3.60	4.73	3.73	5.48	5.21	4.96
0.05	0.07	0.06	0.06	0.06	0.05	0.04	0.07	0.06	0.06	0.08	0.12	0.08	0.02	0.17	0.17	0.17
0.58	0.54	0.52	0.52	0.71	0.51	0.43	0.94	0.7	0.7	0.84	2.45	2.40	1.81	9.73	10.15	9.62
2.17	2.25	2.06	2.29	2.27	1.97	1.83	2.9	2.3	3.22	2.81	4.00	2.50	2.20	6.32	6.68	6.25
2.59	2.39	2.62	2.31	2.36	2.69	2.92	2.74	2.49	2.65	2.68	2.54	3.16	5.75	1.29	1.82	1.66
4.85	4.86	5.12	4.75	4.82	4.84	5.59	5.2	5.27	4.37	4.16	3.04	5.23	1.48	5.58	3.66	4.65
0.14	0.14	0.14	0.14	0.19	0.16	0.12	0.2	0.15	0.12	0.13	0.21	0.27	0.25	0.2	0.21	0.19
1.74	2.99	1.75	3.09	1.39	1.62	1.35	1.48	2.51	2.56	2.44	4.87	0.84	3.14	2.34	2.93	2.38
101.60	100.19	100.07	100.14	99.91	99.87	99.80	98.94	99.52	99.31	99.57	99.74	99.09	99.03	99.3	99.44	99.32
2.58	2.56	2.81	2.50	2.42	2.79	3.12	2.50	2.63	2.44	2.48	1.90	2.72	2.48	2.23	1.85	2.05
1.09	1.08	1.05	1.08	1.13	1.05	1.04	1.01	1.07	0.91	0.95	0.95	1.02	0.98	0.59	0.62	0.63
1.54	1.55	1.44	1.59	1.65	1.44	1.36	1.54	1.53	1.49	1.49	1.88	1.44	1.34	1.43	1.69	1.56
20.6	20.3	20.9	24.8	21.2	20.2	22.2	24.0	21.0	18.0	19.0	19.3	–	–	15.0	15.0	19.0
160	146	181	182	145	143	193	188	218	161	146	151	–	–	189	152	–
182	173	184	174	272	200	189	368	281	205	185	346	–	–	222	250	278
25.7	22.6	23.0	27.5	26.0	23.4	27.0	19.0	22.0	25.0	29.0	24.8	–	–	30.0	24.0	23.0
365	311	338	391	365	312	349	347	306	244	268	169	–	–	108	110	–
18.9	17.8	17.7	20.7	17.9	18.4	19.2	19.0	19.0	19.0	19.0	23.7	–	–	12.0	9.6	21.0
419	406	473	471	648	444	400	1117	744	409	378	508	–	–	455	263	300
8.82	7.81	8.09	9.41	8.63	7.66	8.66	8.70	7.60	6.90	7.30	4.51	–	–	3.40	3.30	–
1.51	1.47	1.49	1.71	1.48	1.54	1.70	1.27	1.12	1.15	1.20	2.28	–	–	1.21	0.92	–
21.5	21.1	19.6	26.2	19.2	21.6	26.9	21.0	21.0	18.0	18.0	23.1	–	–	9.10	8.40	–
3.84	3.56	3.67	3.47	3.97	4.58	6.16	4.50	3.80	3.40	3.50	6.86	–	–	3.60	3.80	–
75.5	74.8	73.6	95.3	77.4	65.0	82.6	72.0	87.0	65.0	73.0	47.5	–	–	20.0	25.0	26.0
148	138	143	180	153	128	169	176	196	143	171	101	–	–	49.0	53.0	52.0
16.1	15.4	15.1	19.3	15.7	13.7	17.4	19.7	22.0	14.0	16.0	10.8	–	–	6.40	6.20	6.80

	58.1	54.5	55.9	67.8	56.7	49.4	61.2	64.0	68.0	47.0	54.0	34.5	–	–	25.0	23.0	27.0
	9.07	8.40	8.42	10.3	8.71	8.00	9.49	8.50	9.10	8.40	9.00	6.35	–	–	5.80	5.00	5.10
	1.31	1.28	1.30	1.57	1.50	1.24	1.24	2.26	1.90	1.27	1.26	1.06	–	–	1.31	1.03	1.20
	6.66	6.19	6.25	7.70	6.57	5.99	7.10	8.20	9.40	6.80	7.40	5.60	–	–	5.20	4.60	5.00
	0.84	0.76	0.77	0.93	0.84	0.77	0.88	0.93	1.05	0.88	0.95	0.78	–	–	0.84	0.67	0.72
	5.15	4.69	4.67	5.77	5.30	4.71	5.30	4.60	4.80	4.80	5.30	5.03	–	–	5.10	4.10	4.40
	1.02	0.91	0.92	1.11	1.01	0.94	1.04	0.87	0.93	0.92	1.05	1.06	–	–	1.07	0.83	0.89
	2.71	2.43	2.36	2.94	2.66	2.50	2.85	2.40	2.60	2.50	2.80	2.94	–	–	3.00	2.40	2.20
	0.39	0.35	0.34	0.43	0.39	0.35	0.41	0.34	0.37	0.36	0.41	0.45	–	–	0.46	0.36	0.35
	2.36	2.11	2.06	2.56	2.38	2.17	2.50	1.90	2.00	2.20	2.50	2.66	–	–	3.00	2.30	2.30
	0.35	0.32	0.31	0.38	0.34	0.33	0.38	0.34	0.36	0.35	0.37	0.41	–	–	0.46	0.36	0.35
	327.8	310.5	315.2	396.0	332.5	283.6	361.3	362.0	405.5	297.5	345.0	219.6	–	–	126.6	128.9	134.3
	15.83	16.47	16.83	17.15	16.06	14.97	16.66	17.49	17.85	14.81	15.60	10.60	–	–	5.62	7.25	7.29
	21.58	23.83	24.09	25.06	21.96	20.21	22.29	25.55	29.33	19.92	19.69	12.04	–	–	4.49	7.33	7.62
	5.23	5.60	5.50	5.81	5.59	5.11	5.47	5.33	6.01	4.87	5.10	4.70	–	–	2.17	3.15	3.21
	0.50	0.52	0.52	0.52	0.58	0.53	0.44	0.82	0.62	0.50	0.46	0.53	–	–	0.72	0.65	0.72

[a] Original data are from Jiang et al. (2005)
[b] Original data are from Xia et al. (1992)
[c] Original data are from Fan et al. (2001b)

rocks postdated the Xiangshan volcanism, but it is clear from present geochronologic data that the age gap might be rather small. Emplacement of the volcanic-intrusive complex took place within a short time period of 135~137 Ma, which is indistinguishable from the age uncertainties of the individual samples.

Petrogenesis of Xiangshan volcanic-intrusive complex

Genetic type

Most igneous rocks of Xiangshan volcanic-intrusive complex are peraluminous (Fig. 4). The samples show a SiO_2 variation between 65.35% and 76.94% and they all have low TiO_2 contents (mostly <0.5 wt%). They are enriched in REE (especially LREE), HFSE (except Nb and Ta, which are relatively depleted) and Ga contents, but are depleted in Ba, Sr, Nd, Ti, P and transition metals. The Ga/Al ratios are high. These geochemical characteristics are comparable to shoshonites (Morrison 1980). In general, all the samples from the volcanic-intrusive complex have an A-type affinity, as indicated by high Ga/Al ratios. They plot in the A-type fields in the 10,000×Ga/Al vs Zr and Nb classification diagrams (not shown, Whalen et al. 1987, 1996; Jiang et al. 2005).

Geothermometry using mineral equilibria (Jiang et al. 2005) and homogenization temperatures of magmatic inclusions (Xia et al. 1992) indicate a high crystallization temperature (>850°C) for the Xiangshan magmas. Trace element geochemistry and Sr–Nd–O isotope systematics imply that the Xiangshan magmas were probably derived from partial melting of Meso-Proterozoic metamorphosed lower-crustal rocks that had been dehydrated during an earlier thermal event (Jiang et al. 2005). Jiang et al. (2005) also suggested a phlogopite-bearing spinel harzburgitic lithospheric mantle source for the mafic microgranular enclave magmas. A back-arc extensional setting related to subduction of the Palaeo-Pacific plate has been favored to explain the petrogenesis of the Xiangshan volcanic-intrusive complex and its mafic microgranular enclaves (Jiang et al. 2005).

Origin of the volcanic-intrusive complex

The Xiangshan volcanic-intrusive complex shows a narrow range of $\varepsilon_{Nd}(T)$ values (−7.4 to −8.8), whereas their initial $^{87}Sr/^{86}Sr$ ratios vary from 0.7087 to 0.7152 (Fig. 8). Previous researchers considered that the Xiangshan volcanic-intrusive complex was derived mainly from partial melting of crustal rocks (e.g. Wang et al. 1991, 1993; Liu et al. 1992; Fan et al. 2001a, b) and derived from a common magmatic source due to their similar Sr–Nd isotopic characteristics (e.g. Shen et al. 1992; Xia et al. 1992; Fan et al. 2001a; Jiang et al. 2005).

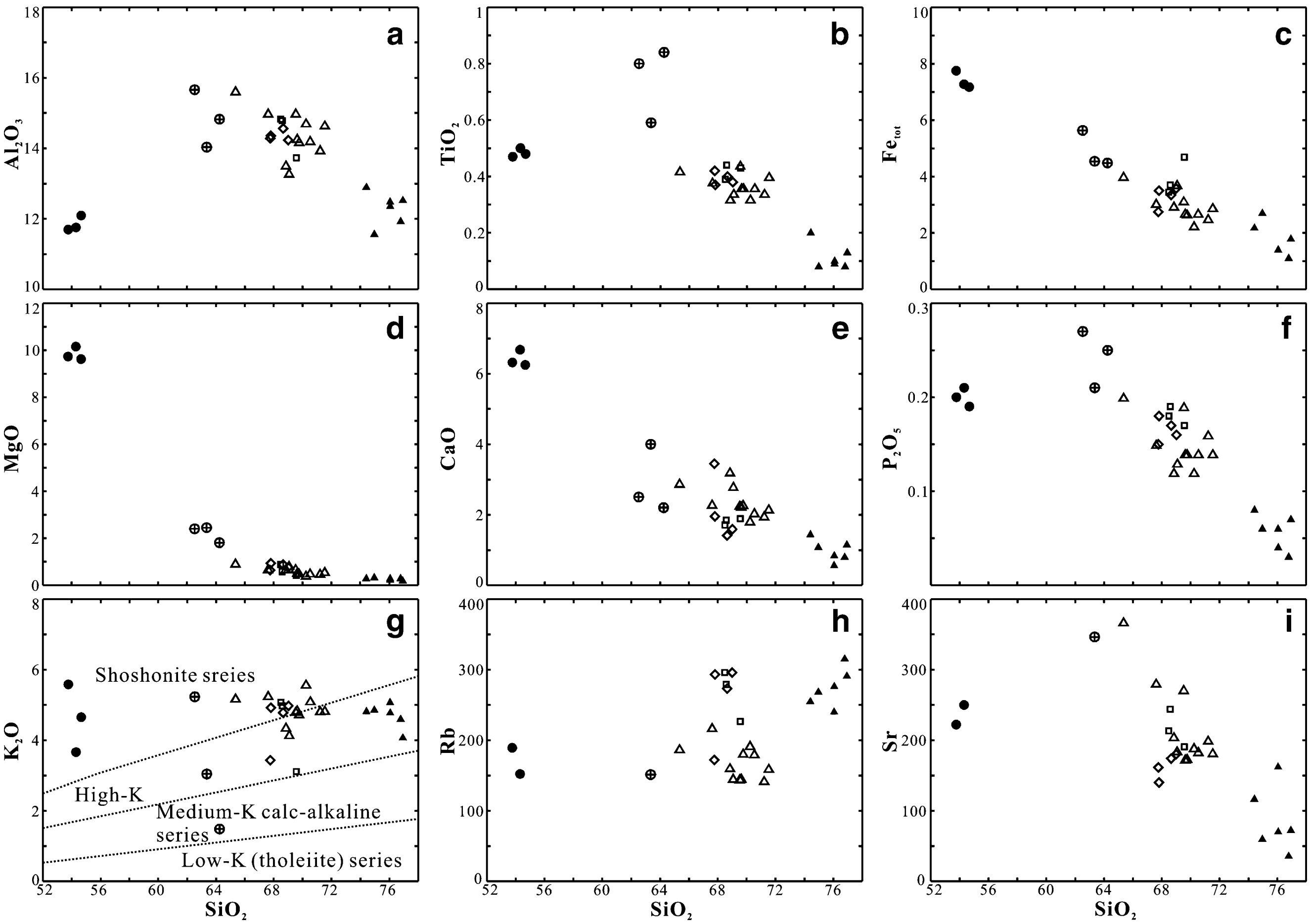

Fig. 5 Chemical variation diagrams for the Xiangshan volcanic-intrusive complex and mafic microgranular enclaves. Symboles are as in Fig. 4

Because of the high closure temperature of the zircon Hf isotopic system (higher than the closure temperature of zircon U–Pb isotopic system; Patchett 1983; Cherniak et al. 1997; Cherniak and Watson 2003), zircon can record the characteristics of different types of source rocks. Therefore, the zircon Hf isotope system has become an important tool to constrain the origin of magmas, especially to decipher processes of crustal evolution and mantle-crust interaction (Griffin et al. 2000, 2002). In all volcanic-intrusive rocks, the approximately 135 Ma old zircons are characterized by negative initial $\varepsilon_{Hf}(t)$ values, ranging from −5.2 to −10.3, with most values concentrated in the range of −7 to −9 (Figs. 7a–e, 9). The negative and unimodally destributed $\varepsilon_{Hf}(t)$ values indicate the same magmatic source for all rocks of the complex and predominantly crust-derived material. Based on the Sr–Nd isotopic composition, Jiang et al. (2005) suggested that the volcanic rocks were probably derived from partial melting of Mesoproterozoic metamorphic rocks including both orthometamorphic and parametamorphic rocks at depth (Fig. 8). A SHRIMP U–Pb zircon age of 1766±19 Ma has been reported for the amphibolites exposed in NW Fujian-SW Zhejiang in the Cathaysia Block (Li et al. 1998). This age is similar to the Nd model ages (1.49 to 1.64 Ga) and Hf model ages (1.55 to 1.83 Ga) (Fig. 9). Therefore, we contend that the Xiangshan volcanic-intrusive complex may have been derived from the remelting of Meso-Palaeoproterozoic metamorphic rocks from Xiangshan basement.

However, it was still unclear whether there is any contribution from mantle-derived magmas. One of the aims of this study was to understand the possible mixing between mantle-derived magmas and crustal melts by applying the Sr–Nd–Hf isotopic systems. For the rhyodacite, rhyodacitic porphyry, porphyritic lava and granite porphyry, similar Nd model ages (1.49 to 1.64 Ga) and Hf model ages (1.55 to 1.83 Ga) have been calculated, indicating a major Paleo-Mesoproterozoic crustal source. In contrast, the quartz monzonitic porphyry has inconsistent Nd and Hf model ages. The quartz monzonitic porphyry has a comparable zircon Hf model age of 1.51 to 1.83 Ga, but a younger whole-rock Nd model age of 1.40 Ga. It appears that the zircon Lu–Hf and whole-rock Sm–Nd

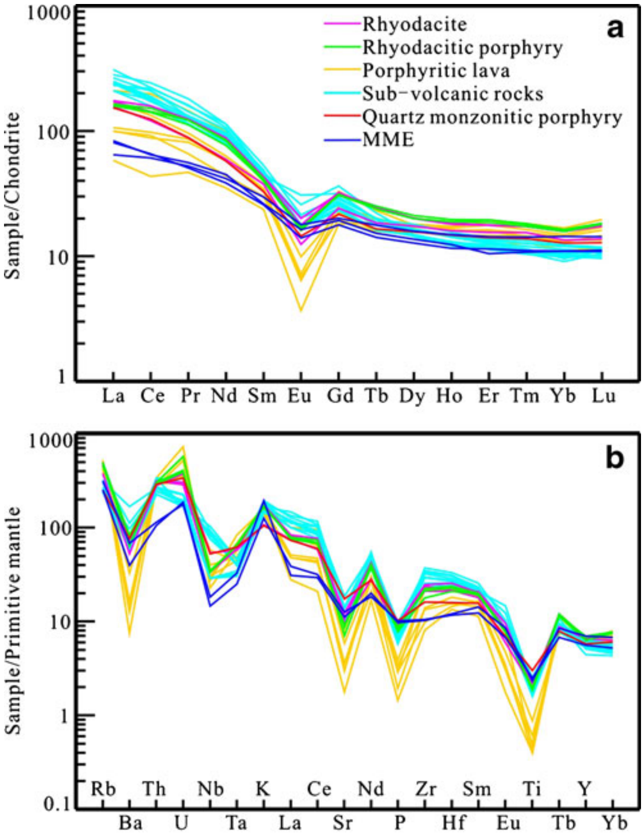

Fig. 6 **a** Chondrite-normalized REE patterns (normalization values are from Boynton 1984) and **b** primitive-mantle-normalized multi-element spidergrams (normalization values are from McDonough and Sun 1995) for Xiangshan volcanic-intrusive complex and mafic microgranular enclaves

isotope systems in quartz monzonitic porphyry were decoupled and evolved in different ways, suggesting the involvement of a major Paleo-Mesoproterozoic crustal source and a subordinate younger mantle component. This occurrence should be basically related to the fact that zircon retains its Hf isotope signature acquired during crystallization from the initial magma, whereas the whole-rock Sm–Nd system was readily equilibrated with the new melt (mafic microgranular enclave magma) and hence gave the lower T_{DM} values. The higher $\varepsilon_{Nd}(T)$ values of −5.7 for quartz monzonitic porphyry also indicates the involvement of mantle-derived magma, although we also cannot rule out the possibility of remelting of larger amounts of older basaltic underplated material.

Fractionation processes

On binary major element vs SiO_2 variation diagrams, compositional gaps are common features of the complex, whereas major oxides (except K_2O and Na_2O) show linear trends. The REE of the complex are characterized by significant enrichment of LREE relative to HREE, and the REE patterns for complex are actually inhomogeneous. The granite porphyry has the highest LREE content and lowest HREE content (14.81 > LREE/HREE > 17.85), its distribution curves showing significantly steeper trends than other rocks (Fig. 6a). Porphyritic lava shows the lowest LREE content and has the largest negative Eu anomalies (0.42 > Eu/Eu* > 0.18) (Fig. 6a). The primitive mantle-normalized multi-element diagrams (McDonough and Sun 1995) (Fig. 6b) show significant negative Ba, Sr, P and Ti anomalies in the porphyritic lava, though the complex has relatively similar patterns to the primitive mantle-normalized element spidergrams.

Taking into account that magmatic activity in the Xiangshan volcanic-intrusive complex is contemporaneous based on the precise zircon U–Pb ages of this study, and they have similar whole rock Sr–Nd and zircon Hf isotopic compositions, fractional crystallization, rather than magma mixing or partial melting of heterogeneous sources during the formation of these rocks, is favored to explain the diversity of the element variations. This is supported by depletions in Ba, Sr, Nb, P, Ti and Eu shown in the spidergrams (Fig. 6). Strong Eu depletion requires extensive fractionation of plagioclase and/or K-feldspar. Fractionation of plagioclase would result in negative Sr and Eu anomalies, and that of K-feldspar would produce negative Eu and Ba anomalies.

In log–log diagrams of Ba vs Sr, Ba vs Rb, Ba/Sr vs Sr and Rb/Sr vs Sr (Fig. 10), it appears that the granite porphyry is less influenced by crystal fractionation, and could be regarded as the initial composition of the melt. Ba changes little in the crystallization of rhyodacite, rhyodacitic porphyry and granite porphyry, but decreases rapidly in the crystallization of porphyritic lava. This is explained by the separation of plagioclase in the crystallization stage of rhyodacite, rhyodacitic porphyry, and by fractionation of K-feldspar in the crystallization stage of porphyritic lava. In addition to major phases, accessory minerals seem to have controlled much of the REE variation. The decrease of LREE with increasing SiO_2 suggests a separation of minerals with high LREE, such as apatite, zircon and allanite, which are important accessory minerals in these rocks. According to the diagram of $(La/Yb)_N$ vs La (Fig. 11), the variation of REE contents seems to be controlled by fractionation of allanite during magmatic evolution.

A new integrated model for the origin of the Xiangshan volcanic-intrusive complex

A model for the origin of the Xiangshan volcanic-intrusive complex has been previously proposed by Jiang et al. (2005). However, based on the geochronology and petrological data

Table 5 Nd and Sr isotopic systematics of the volcanic-intrusive complex and mafic microgranular enclaves from Xiangshan, SE China

Sample	Rock type	Age (Ma)	Sm	Nd	$^{147}Sm/^{144}Nd$	$^{143}Nd/^{144}Nd$	2σ	Sm/Nd	I_{Nd}	$\varepsilon_{Nd}(0)$	$\varepsilon_{Nd}(t)$	T_{DM}	T_{DM}^{C}	Rb	Sr	$^{87}Rb/^{86}Sr$	$^{87}Sr/^{86}Sr$	2σ	I_{Sr}
XS-30-1	Rhyodacite	135	7.30	35.4	0.1246	0.512197	33	0.21	0.512087	−8.60	−7.36	1630	1528	227	190	3.4447	0.718530	4	0.711915
X9-18a	Rhyodacite	135	8.32	37.9	0.1325	0.512196	3	0.22	0.512079	−8.62	−7.52	1790	1540	263	181	4.2054	0.718183	9	0.710108
XS-30-3	Rhyodacitic porphyry	135	7.03	35.5	0.1198	0.512193	2	0.20	0.512087	−8.68	−7.36	1555	1527	172	161	3.0830	0.720964	2	0.715057
X9-20a	Rhyodacitic porphyry	135	7.86	38.0	0.1250	0.512161	6	0.21	0.512051	−9.30	−8.07	1700	1585	256	113	6.5600	0.721085	14	0.708516
XS-29-1	Porphyritic lava	132	7.31	37.9	0.1164	0.512157	4	0.19	0.512056	−9.38	−8.03	1556	1579	254	116	6.3383	0.722225	5	0.710297
XS-59	Porphyritic lava	135	5.83	26.3	0.1341	0.512189	6	0.22	0.512070	−8.76	−7.68	1839	1553	290	71.8	11.7036	0.732225	5	0.709751
X9-21a	Porphyritic lava	135	5.79	20.5	0.1703	0.512188	8	0.28	0.512037	−8.78	−8.33	3365	1606	299	42.7	20.2294	0.750231	12	0.711385
X9-22a	Porphyritic lava	135	7.11	31.2	0.1376	0.512199	8	0.23	0.512077	−8.56	−7.55	1905	1543	275	70.3	11.3217	0.733224	8	0.711483
X9-24a	Porphyritic lava	135	6.97	32.5	0.1297	0.512182	8	0.21	0.512067	−8.90	−7.74	1756	1558	290	71.2	11.7801	0.731717	11	0.709096
XS-07	Granite porphyry	137	9.07	58.1	0.0944	0.512167	2	0.16	0.512083	−9.19	−7.41	1257	1532	160	182	2.5405	0.716993	3	0.712060
XS-08	Granite porphyry	137	8.40	54.5	0.0930	0.512172	4	0.15	0.512089	−9.09	−7.29	1237	1523	146	173	2.4375	0.718298	2	0.713565
XS-09	Granite porphyry	137	8.42	55.9	0.0910	0.512192	8	0.15	0.512111	−8.70	−6.86	1191	1488	181	184	2.8418	0.717198	9	0.711680
XS-10	Granite porphyry	137	10.3	67.8	0.0919	0.512159	8	0.15	0.512077	−9.34	−7.52	1241	1542	182	174	3.0192	0.720515	2	0.714653
XS-12	Granite porphyry	137	8.71	56.7	0.0929	0.512098	11	0.15	0.512015	−10.53	−8.73	1328	1639	145	272	1.5467	0.715358	3	0.712355
XS-13	Granite porphyry	137	8.00	49.4	0.0977	0.512168	2	0.16	0.512081	−9.17	−7.45	1292	1536	143	200	2.0662	0.717089	4	0.713077
XS-43	Granite porphyry	137	9.49	61.2	0.0937	0.512157	2	0.16	0.512073	−9.38	−7.59	1262	1547	193	189	2.9425	0.717943	2	0.712230
SB-1a	Granite porphyry	137	9.50	61.2	0.0938	0.512165	6	0.16	0.512081	−9.23	−7.43	1253	1535	178	205	2.5018	0.715619	7	0.710762
XS-63	Quartz monzonitic porphyry	136	6.35	34.5	0.1113	0.512268	6	0.18	0.512169	−7.22	−5.74	1314	1396	151	346	1.2624	0.712489	4	0.710049
SB-5b	Mafic microgranular enclave	135	4.84	26.5	0.1106	0.512346	14	0.18	0.512248	−5.70	−4.21	1190	1272	139	223	1.8014	0.711515	12	0.708058

[a] Original data are from Jiang et al. (2005)

[b] Original data are from Fan et al. (2001b)

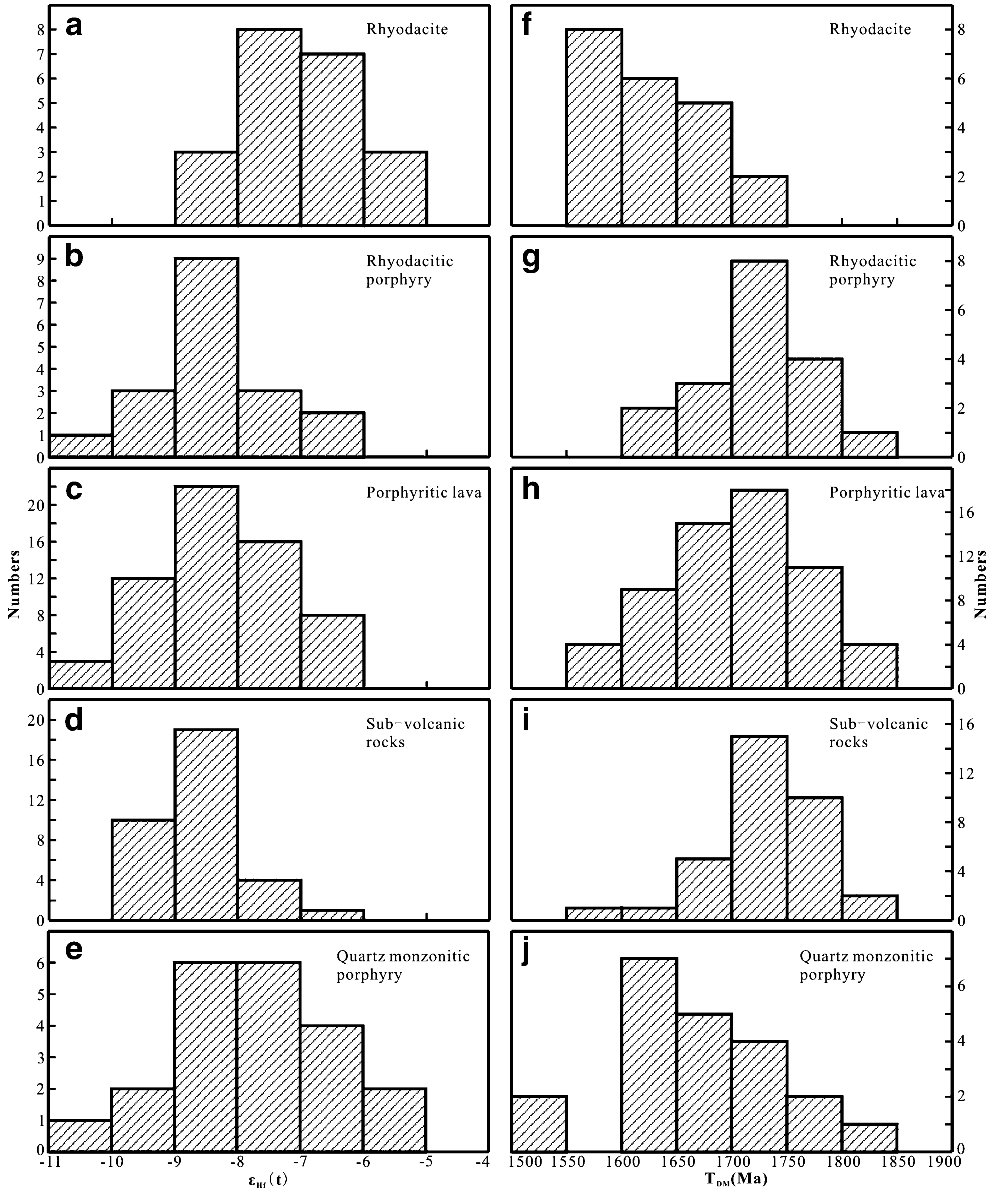

Fig. 7 Histogram of $\varepsilon_{Nd}(T)$ values and Hf model ages for the Xianghsan volcanic-intrusive complex

presented in this paper, this model needs significant modification. The volcanic activity of Xiangshan occurred during the Early Cretaceous (about 135 Ma), rather than Late Jurassic to Early Cretaceous (158 to 135 Ma), which was cited in the Jiang et al. (2005)'s model.

Moreover, there are lamprophyre dykes in the volcanic-intrusive complex, showing that the mafic magmas were emplaced at the felsic magma emplacement levels. In the Jiang et al. (2005) model, the mafic microgranular enclaves were generated in the lower crust where the felsic magma chamber formed. Furthermore, although the enclaves are darker and finer-grained than their host granitoids, most are intermediate to felsic in composition. The relatively fine-grained microstructures indicate relatively rapid crystallization. The enclave magma crystallized more rapidly than the felsic magma (Zeck 1970), once thermal equilibrium has been established. The felsic and mafic magmas could remain separate (Yoder 1973), particularly if small volumes of more mafic magma are enclosed in large volumes of felsic magma and if mixing is minimal (Kouchi and Sunagawa 1983), because chilling increases the viscosity of the more mafic globules, as well as promoting viscosity during rapid crystallization. Mafic microgranular enclaves typically show little or no evidence of disintegration after their injection into felsic magma, and the surrounding granitoid is generally not obviously modified. Both the compositional gap and discontinuous compositional trend between the mafic microgranular enclaves and their host

Table 6 LA-MC-ICP-MS in situ analysis of zircon Lu-Hf isotopic composition of volcanic-intrusive complex from Xiangshan, SE China

Spot	Age	$^{176}Yb/^{177}Hf$	$^{176}Lu/^{177}Hf$	$^{176}Hf/^{177}Hf$		$\varepsilon_{Hf}(0)$	$\varepsilon_{Hf}(t)$	2σ	T_{DM1}/(Ma)	T_{DM}^{C}/(Ma)	$f_{Lu/Hf}$
	(Ma)	Ratio	Ratio	Ratio	2σ						
XS-05 Porphyritic lava											
XS-05-1	133	0.043249	0.000986	0.282479	0.000021	−10.4	−7.5	0.7	1093	1660	−0.97
XS-05-2	131	0.047360	0.001338	0.282455	0.000025	−11.2	−8.4	0.9	1137	1715	−0.96
XS-05-3	128	0.038116	0.001186	0.282410	0.000029	−12.8	−10.1	1.0	1196	1817	−0.96
XS-05-4	132	0.038997	0.000947	0.282508	0.000024	−9.3	−6.5	0.8	1050	1595	−0.97
XS-05-5	133	0.031127	0.000827	0.282448	0.000021	−11.5	−8.6	0.8	1131	1727	−0.98
XS-05-6	130	0.041716	0.000945	0.282473	0.000020	−10.6	−7.8	0.7	1100	1675	−0.97
XS-05-7	137	0.044560	0.001016	0.282480	0.000021	−10.3	−7.4	0.7	1092	1654	−0.97
XS-05-8	124	0.047473	0.001106	0.282489	0.000020	−10.0	−7.4	0.7	1082	1643	−0.97
XS-05-9	135	0.036665	0.001054	0.282465	0.000024	−10.9	−8.0	0.8	1115	1690	−0.97
XS-05-10	137	0.071406	0.001893	0.282445	0.000023	−11.5	−8.7	0.8	1168	1736	−0.94
XS-05-11	128	0.041717	0.000970	0.282462	0.000020	−11.0	−8.2	0.7	1116	1700	−0.97
XS-05-12	136	0.031405	0.000730	0.282433	0.000021	−12.0	−9.1	0.7	1150	1759	−0.98
XS-05-13	135	0.063813	0.001958	0.282446	0.000023	−11.5	−8.7	0.8	1169	1736	−0.94
XS-05-14	135	0.053587	0.001597	0.282437	0.000026	−11.8	−9.0	0.9	1170	1753	−0.95
XS-05-15	134	0.031205	0.000870	0.282485	0.000020	−10.1	−7.3	0.7	1081	1645	−0.97
XS-05-16	136	0.043970	0.001039	0.282466	0.000015	−10.8	−7.9	0.5	1113	1687	−0.97
XS-05-17	138	0.043087	0.001004	0.282511	0.000016	−9.2	−6.3	0.6	1048	1585	−0.97
XS-05-18	133	0.029092	0.000745	0.282484	0.000016	−10.2	−7.3	0.6	1079	1646	−0.98
XS-05-19	140	0.066510	0.002041	0.282453	0.000020	−11.3	−8.4	0.7	1162	1720	−0.94
XS-05-20	137	0.032470	0.000867	0.282480	0.000018	−10.3	−7.4	0.6	1088	1654	−0.97
XS-05-21	140	0.043798	0.001104	0.282462	0.000020	−11.0	−8.0	0.7	1121	1694	−0.97
XS-05-22	137	0.052654	0.001267	0.282446	0.000016	−11.5	−8.6	0.6	1147	1731	−0.96
XS-29-1 Porphyritic lava											
XS29-1-1.1	133	0.034238	0.000792	0.282479	0.000016	−10.4	−7.5	0.6	1088	1659	−0.98
XS29-1-2.1	135	0.038980	0.000869	0.282442	0.000016	−11.7	−8.8	0.6	1141	1740	−0.97
XS29-1-3.1	133	0.033488	0.000837	0.282438	0.000020	−11.8	−9.0	0.7	1146	1750	−0.97
XS29-1-4.1	134	0.031162	0.000738	0.282442	0.000017	−11.7	−8.8	0.6	1137	1739	−0.98
XS29-1-5.1	133	0.027111	0.000720	0.282421	0.000013	−12.4	−9.6	0.5	1166	1787	−0.98
XS29-1-6.1	134	0.037021	0.000995	0.282435	0.000017	−11.9	−9.1	0.6	1154	1755	−0.97
XS29-1-7.1	133	0.024072	0.000681	0.282456	0.000015	−11.2	−8.3	0.5	1116	1709	−0.98
XS29-1-8.1	132	0.053082	0.001496	0.282402	0.000017	−13.1	−10.3	0.6	1216	1832	−0.95
XS29-1-9.1	131	0.036654	0.000995	0.282416	0.000019	−12.6	−9.8	0.7	1182	1801	−0.97
XS29-1-10.1	131	0.027215	0.000784	0.282433	0.000016	−12.0	−9.2	0.5	1151	1761	−0.98

XS29-1-11.1	126	0.027848	0.000687	0.282435	0.000019	−11.9	−9.2	0.7	1145	1758	−0.98
XS29-1-12.1	125	0.032325	0.000926	0.282456	0.000018	−11.2	−8.5	0.6	1123	1714	−0.97
XS29-1-13.1	130	0.033102	0.000947	0.282416	0.000018	−12.6	−9.8	0.6	1179	1800	−0.97
XS29-1-14	132	0.029943	0.000784	0.282423	0.000015	−12.3	-9.5	0.5	1164	1782	−0.98
XS29-1-15	132	0.036765	0.001058	0.282403	0.000015	−13.1	−10.2	0.5	1202	1829	−0.97
XS29-1-16	132	0.040556	0.000974	0.282441	0.000020	−11.7	−8.9	0.7	1146	1744	−0.97
XS29-1-17	132	0.041997	0.001020	0.282467	0.000022	−10.8	−8.0	0.8	1111	1687	−0.97
XS-59 Porphyritic lava											
XS-59-1	136	0.028471	0.000625	0.282419	0.000019	−12.5	−9.6	0.7	1166	1789	−0.98
XS-59-2	139	0.042264	0.000950	0.282423	0.000021	−12.3	−9.4	0.7	1169	1779	−0.97
XS-59-3	137	0.041019	0.000902	0.282454	0.000015	−11.2	−8.3	0.5	1125	1712	−0.97
XS-59-4	136	0.028409	0.000642	0.282442	0.000018	−11.7	−8.8	0.6	1135	1738	−0.98
XS-59-5	135	0.036704	0.000851	0.282494	0.000017	−9.8	−6.9	0.6	1067	1623	−0.97
XS-59-6	133	0.035993	0.000846	0.282460	0.000014	−11.0	−8.2	0.5	1114	1699	−0.97
XS-59-7	138	0.050672	0.001258	0.282501	0.000016	−9.6	−6.7	0.6	1069	1609	−0.96
XS-59-8	135	0.045099	0.001108	0.282472	0.000017	−10.6	−7.7	0.6	1106	1674	−0.97
XS-59-9	141	0.080666	0.001933	0.282468	0.000013	−10.8	−7.8	0.5	1137	1685	−0.94
XS-59-10	133	0.034195	0.000815	0.282442	0.000016	−11.7	−8.8	0.6	1139	1740	−0.98
XS-59-11	134	0.063359	0.001463	0.282488	0.000018	−10.1	−7.3	0.7	1094	1642	−0.96
XS-59-12	135	0.042589	0.001058	0.282463	0.000014	−10.9	−8.1	0.5	1118	1695	−0.97
XS-59-13	107	0.051568	0.001281	0.282453	0.000017	−11.3	−9.0	0.6	1138	1734	−0.96
XS-59-14	135	0.067249	0.001804	0.282471	0.000017	−10.7	−7.9	0.6	1129	1681	−0.95
XS-59-15	136	0.027644	0.000656	0.282492	0.000016	−9.9	−7.0	0.6	1065	1626	−0.98
XS-59-16	133	0.051048	0.001298	0.282508	0.000016	−9.3	−6.5	0.6	1061	1597	−0.96
XS-59-17	135	0.054307	0.001330	0.282495	0.000014	−9.8	−6.9	0.5	1080	1624	−0.96
XS-59-18	132	0.029224	0.000744	0.282455	0.000013	−11.2	−8.4	0.4	1119	1712	−0.98
XS-59-19	130	0.018465	0.000487	0.282489	0.000013	−10.0	−7.2	0.5	1065	1637	−0.99
XS-59-20	135	0.049455	0.001322	0.282457	0.000019	−11.1	−8.3	0.7	1134	1709	−0.96
XS-59-22	135	0.036836	0.000952	0.282510	0.000017	−9.3	−6.4	0.6	1048	1588	−0.97
XS-59-23	135	0.048692	0.001305	0.282449	0.000016	−11.4	−8.6	0.6	1145	1727	−0.96
XS-12 Granite porphyry											
XS12-1.1	136	0.041978	0.001001	0.282518	0.000019	−9.0	−6.1	0.7	1038	1571	−0.97
XS12-2.1	140	0.050282	0.001209	0.282454	0.000016	−11.2	−8.3	0.6	1134	1711	−0.96
XS12-3.1	137	0.026171	0.000651	0.282475	0.000017	−10.5	−7.5	0.6	1088	1663	−0.98
XS12-4.1	137	0.024618	0.000695	0.282425	0.000015	−12.3	−9.3	0.5	1159	1775	−0.98
XS12-5.1	137	0.033603	0.000898	0.282453	0.000016	−11.3	−8.4	0.6	1126	1714	−0.97
XS12-6.1	139	0.022494	0.000630	0.282440	0.000018	−11.7	−8.8	0.6	1137	1740	−0.98
XS12-7.1	137	0.024444	0.000670	0.282449	0.000013	−11.4	−8.5	0.5	1126	1723	−0.98

Table 6 (continued)

Spot	Age	$^{176}Yb/^{177}Hf$	$^{176}Lu/^{177}Hf$	$^{176}Hf/^{177}Hf$		$\varepsilon_{Hf}(0)$	$\varepsilon_{Hf}(t)$	2σ	T_{DM1}/(Ma)	T_{DM}^{C}/(Ma)	$f_{Lu/Hf}$
	(Ma)	Ratio	Ratio	Ratio	2σ						
XS12-8.1	138	0.044844	0.001260	0.282409	0.000016	−12.8	−9.9	0.6	1200	1813	−0.96
XS12-9.1	136	0.032115	0.000974	0.282436	0.000026	−11.9	−9.0	0.9	1152	1752	−0.97
XS12-10.1	137	0.065317	0.001510	0.282471	0.000019	−10.6	−7.8	0.7	1119	1678	−0.95
XS12-11.1	135	0.024021	0.000614	0.282453	0.000021	−11.3	−8.4	0.7	1118	1714	−0.98
XS12-11.2	134	0.041806	0.001054	0.282463	0.000019	−10.9	−8.1	0.7	1117	1694	−0.97
XS12-12	137	0.025980	0.000696	0.282444	0.000015	−11.6	−8.7	0.5	1133	1732	−0.98
XS12-13	137	0.036280	0.000949	0.282427	0.000015	−12.2	−9.3	0.5	1164	1771	−0.97
XS12-14	137	0.037540	0.000945	0.282435	0.000018	−11.9	−9.0	0.6	1153	1754	−0.97
XS12-16	137	0.045121	0.001139	0.282447	0.000019	−11.5	−8.6	0.7	1142	1729	−0.97
XS12-17	137	0.033596	0.000865	0.282447	0.000015	−11.5	−8.6	0.5	1134	1728	−0.97
XS12-18	137	0.040017	0.000936	0.282488	0.000019	−10.0	−7.1	0.7	1078	1636	−0.97
XS12-19	137	0.021553	0.000540	0.282467	0.000015	−10.8	−7.8	0.5	1096	1681	−0.98
XS-30-2 Granite porphyry											
XS-30-2-1	133	0.038227	0.000953	0.282445	0.000012	−11.6	−8.7	0.4	1139	1734	−0.97
XS-30-2-2	139	0.030701	0.000764	0.282414	0.000011	−12.6	−9.7	0.4	1176	1797	−0.98
XS-30-2-3	137	0.041681	0.001027	0.282461	0.000012	−11.0	−8.1	0.4	1119	1697	−0.97
XS-30-2-4	138	0.027307	0.000679	0.282437	0.000012	−11.9	−8.9	0.4	1142	1748	−0.98
XS-30-2-5	140	0.043101	0.001106	0.282441	0.000011	−11.7	−8.7	0.4	1149	1739	−0.97
XS-30-2-6	139	0.033674	0.000877	0.282443	0.000012	−11.6	−8.7	0.4	1139	1734	−0.97
XS-30-2-7	139	0.034729	0.000967	0.282447	0.000015	−11.5	−8.5	0.5	1137	1726	−0.97
XS-30-2-9	130	0.031710	0.000798	0.282447	0.000026	−11.5	−8.7	0.9	1131	1730	−0.98
XS-30-2-10	134	0.080247	0.001987	0.282435	0.000015	−11.9	−9.2	0.5	1186	1762	−0.94
XS-30-2-11	134	0.041533	0.001049	0.282412	0.000016	−12.7	−9.9	0.6	1189	1808	−0.97
XS-30-2-12	136	0.035522	0.000898	0.282425	0.000015	−12.3	−9.4	0.5	1165	1776	−0.97
XS-30-2-13	133	0.037174	0.000901	0.282431	0.000013	−12.0	−9.2	0.5	1157	1764	−0.97
XS-30-2-14	137	0.050172	0.001229	0.282431	0.000017	−12.0	−9.2	0.6	1167	1764	−0.96
XS-30-2-15	137	0.046434	0.001177	0.282440	0.000011	−11.7	−8.9	0.4	1153	1745	−0.96
XS-30-2-16	137	0.027086	0.000718	0.282433	0.000019	−12.0	−9.1	0.7	1149	1758	−0.98
XS-63 Quartz monzonitic porphyry											
XS63-1.1	131	0.022225	0.000607	0.282482	0.000011	−10.3	−7.4	0.4	1078	1652	−0.98
XS63-2.1	133	0.038219	0.001042	0.282504	0.000014	−9.5	−6.6	0.5	1059	1603	−0.97
XS63-3.1	136	0.032424	0.000825	0.282543	0.000012	−8.1	−5.2	0.4	998	1514	−0.98
XS63-4.1	135	0.036430	0.000936	0.282426	0.000011	−12.2	−9.4	0.4	1165	1774	−0.97
XS63-4.2	135	0.029800	0.000768	0.282478	0.000012	−10.4	−7.5	0.4	1088	1660	−0.98

XS63-5.1	136	0.032693	0.000852	0.282486	0.000011	−10.1	−7.2	0.4	1079	1642	−0.97
XS63-5.2	442	0.022999	0.000579	0.281860	0.000011	−32.3	−22.7	0.4	1933	2832	−0.98
XS63-6.1	130	0.026936	0.000626	0.282461	0.000013	−11.0	−8.2	0.5	1107	1698	−0.98
XS63-7.1	135	0.031594	0.000864	0.282491	0.000010	−9.9	−7.0	0.4	1072	1630	−0.97
XS63-8.1	137	0.033640	0.000951	0.282486	0.000014	−10.1	−7.2	0.5	1081	1641	−0.97
XS63-9.1	154	0.004096	0.000094	0.282529	0.000013	−8.6	−5.2	0.4	999	1531	−1.00
XS63-10.1	135	0.030512	0.000851	0.282461	0.000014	−11.0	−8.1	0.5	1114	1698	−0.97
XS63-11.1	144	0.080510	0.002595	0.282402	0.000022	−13.1	−10.2	0.8	1253	1832	−0.92
XS63-11.2	138	0.053273	0.001598	0.282424	0.000019	−12.3	−9.4	0.7	1189	1782	−0.95
XS63-12.1	137	0.043597	0.001397	0.282439	0.000024	−11.8	−8.9	0.8	1161	1748	−0.96
XS63-12.2	130	0.033523	0.000931	0.282441	0.000028	−11.7	−8.9	1.0	1144	1744	−0.97
XS63-13.1	137	0.058728	0.001775	0.282460	0.000028	−11.0	−8.2	1.0	1142	1703	−0.95
XS63-14.1	136	0.073257	0.002058	0.282505	0.000014	−9.5	−6.7	0.5	1087	1607	−0.94
XS63-14.2	136	0.083784	0.002210	0.282496	0.000012	−9.8	−7.0	0.4	1104	1626	−0.93
XS63-15	136	0.040716	0.001328	0.282480	0.000019	−10.3	−7.5	0.7	1101	1657	−0.96
XS63-16	136	0.041148	0.001182	0.282494	0.000012	−9.8	−7.0	0.4	1077	1625	−0.96
XS63-17	136	0.036247	0.000941	0.282438	0.000012	−11.8	−8.9	0.4	1149	1748	−0.97

volcanic rocks at Xiangshan suggest minimal scale mixing between mafic microgranular enclave magma and their host granitoid magma (Fig. 5). Besides, disintegration of enclaves should disseminate finer-grained material (Vernon 1984) than is typical of granite porphyry at Xiangshan. Furthermore, the report of lamprophyric dykes (Fan et al. 2005), resembling enclaves in adjacent granitoids suggests that enclave magmas can exist either independently of, or as a separate layer in, their host granitoid magma bodies. So the compositional variety of the enclave magmas was produced before their injection and away from the exposed site of final mingling. Consequently, we propose a two-magma-chamber model for the development of the Xiangshan volcanic-intrusive complex and mafic microgranular enclaves. The formation of the Xiangshan mafic microgranular enclaves can be explained by the injection of the mafic magma from a deep seated magma chamber toward the hypabyssal felsic magma chamber.

Based on the petrological and geochemical data presented in this paper, a new integrated model for the origin of the Xiangshan volcanic complex is proposed, as shown in Fig. 12a–d. During the Cretaceous, it is suggested that an extensional environment predominated in SE China (Li 2000), and Zhou and Li (2000) have suggested a model associated with the Palaeo-Pacific plate subduction and underplating of mafic magmas for the origin of Late Mesozoic igneous rocks in SE China. At Early Cretaceous (about 135 Ma) time, the dip angle of the subducted slab increased, resulting in oceanward migration of the active magmatic zone (Fig. 12a) (Zhou and Li 2000; Jiang et al. 2005). At the same time, back-arc extension, and upwelling of the astenthenosphere, as a consequence of slab roll-back, resulted in partial melting of the lithospheric mantle, generating the high-Mg potassic magmas in the lower crust (Jiang et al. 2005). Underplating of these anomalously high-temperature (>1,200°C) (Jiang et al. 2005) melts into the crustal source region induced partial melting. Such crustal melts diapirs rose and assembled to form hypabyssal felsic magma chambers, which then erupted to form the Xiangshan volcanic rocks (such as rhyodacite, and followed by the fractionation crystallization of plagioclase and allanite, Fig. 12b) and the Xiangshan intrusive rock (porphyritic lava, and followed by the fractional crystallization of K-feldspar and allanite, Fig. 12c). The plutonic high-Mg potassic magma chamber and hypabyssal felsic magma chamber were connected throughout the extensional tectonics. High-Mg potassic magmas from the plutonic magma chamber injected into the hypabyssal felsic magma chamber through the extensional channel or faulted structures. The composition of the high-Mg potassic magma may have been changed by concurrent hybridization and assimilation of partial melts over the large depth range during the protracted upward percolation in the plexus of crustal conduits, and mafic microgranular

Table 7 Lu–Hf isotopic character for zircons from the Xiangshan volcanic-intrusive complex

Lithology	$\varepsilon_{Hf}(T)$		T_{DM}^{C}		Reference
	Range	Average	Range (Ma)	Average	
Rhyodacite	–5.7~–8.5	–7.0	1550~1720	1630	Yang et al. (2010)
Rhyodacitic porphyry	–6.9~–10.1	–8.5	1621~1823	1721	Yang et al. (2010)
Porphyritic lava	–6.3~–10.3	–8.3	1585~1832	1706	This study
Subvolcanic rocks	–6.1~–9.9	–8.6	1571~1813	1731	This study
Quartz monzonitic porphyry	–5.2~–10.2	–7.7	1514~1832	1672	This study

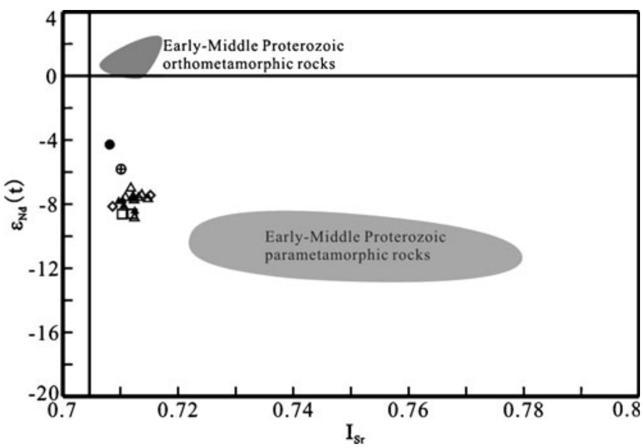

Fig. 8 Initial $^{87}Sr/^{86}Sr$ vs $\varepsilon_{Nd}(t)$ diagram for the volcanic-intrusive complex and mafic microgranular enclaves from the Xiangshan. The Sr and Nd isotope data for orthometamorphic and parametamorphic rocks are from Yuan et al. (1991) and Hu et al. (1999), I_{Sr} and $\varepsilon_{Nd}(T)$ were calculated at 135 Ma for these metamorphic rocks. Symboles are as in Fig. 4

enclaves appear to crystallize at granitoid host magma emplacement levels (Fig. 12d).

Conclusions

On the basis of the integrated geochronological, geochemical and Sr–Nd–Hf isotopic analyses of the Xiangshan volcanic-intrusive complex, SE China, the following scenario can be outlined:

(1) U–Pb zircon dating of the volcanic-intrusive complex from Xiangshan provides insights into the extrusive and intrusive activity at Xiangshan, which took place within a short time span (135–137 Ma), and overlaps with the peak episode of an extensional tectonic regime during the Cretaceous in SE China.

(2) Geochemical data indicate that all the samples from the Xiangshan volcanic-intrusive complex have A-type affinities. Their similar whole rock Sr–Nd and zircon Hf isotopic data suggest that igneous rocks in the Xiangshan volcanic-intrusive complex have the same magmatic source, and were derived mainly from Paleo-Mesoproterozoic crustal rocks, without signifi-

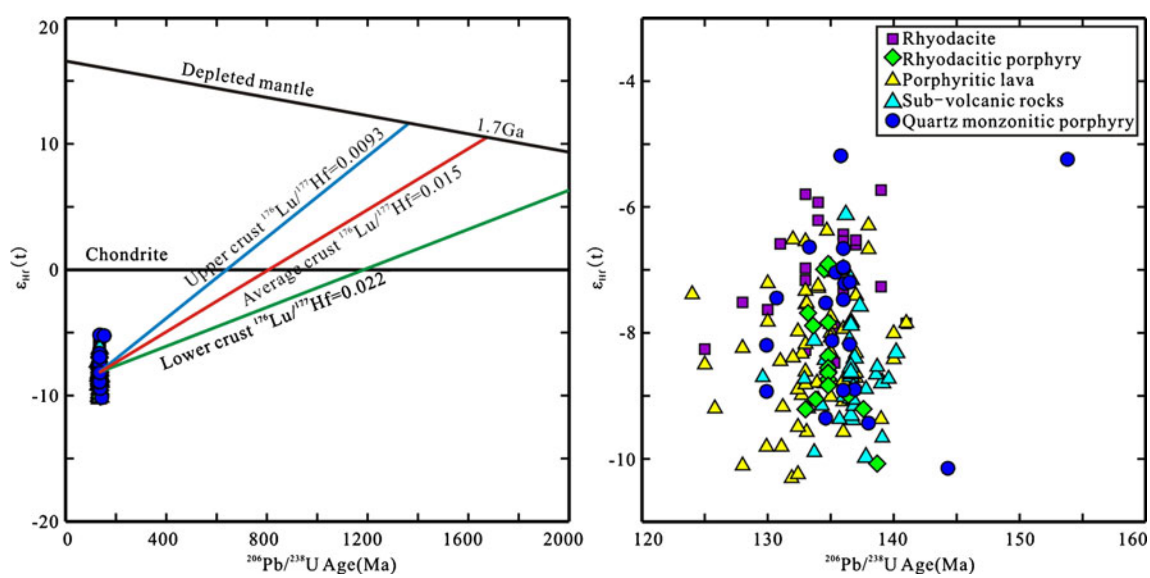

Fig. 9 $^{206}Pb/^{238}U$ ages vs $\varepsilon_{Hf}(t)$ of zircons from the Xiangshan volcanic-intrusive complex

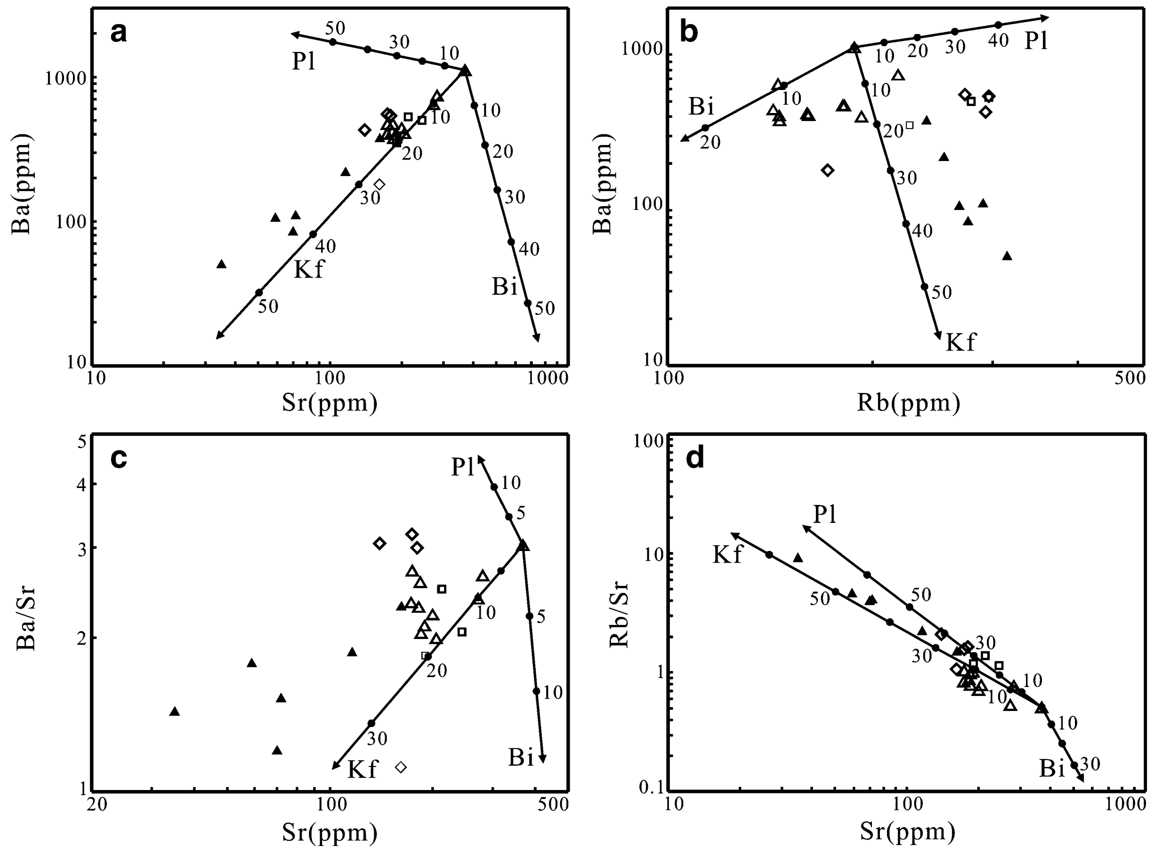

Fig. 10 **a** Ba vs Sr, **b** Ba vs Rb, **c** Ba/Sr vs Sr and **d** Rb/Sr vs Sr diagrams showing that fractionation of plagioclase plays an important role in the rhyodacite (and rhyodacitic porphyry) stage of differentiation; whereas in the prophyritic lava stage, separation of K-feldspar appears to have controlled the variation of these elements. Partition coefficients of Rb, Sr and Ba are from Philpotts and Schnetzler (1970). Symboles are as in Fig. 4

cant addition of mantle-derived magma (except quartz monzonitic porphyry, which has higher $\varepsilon_{Nd}(T)$ values of −5.8, and may indicate the involvement of a subordinate younger mantle-derived magma for its magmatic origin). Geochemical studies indicate that rocks from the complex have variable REE patterns and they show negative anomalies of Ba, Nb, Sr, P, Eu and Ti in spidergrams, suggesting that these rocks have undergone advanced fractional crystallization with separation of plagioclase, K-feldspar and accessory minerals such as allanite.

(3) Detailed petrographic, chemical, and isotope studies of the Xiangshan volcanic complex and its mafic microgranular enclaves provide information on their genesis and evolution. Our model interprets this Cretaceous complex as forming in an extensional and back-arc environment. The formation of the Xiangshan mafic microgranular enclaves can be explained with the injection of mafic magma from a deep seated magma chamber into a hypabyssal felsic magma chamber at a higher emplacement level in the crust.

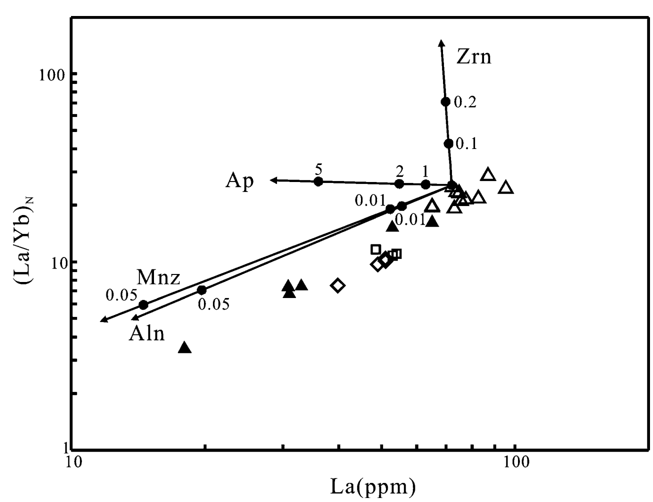

Fig. 11 $(La/Yb)_N$ vs La diagram showing the change of REE patterns by separation of accessory minerals, especially allanite and apatite. Partition coefficients are from Fujimaki (1986) for apatite, Mahood and Hildreth (1983) for zircon and allanite, and Yurimoto et al. (1990) for monazite. Symboles are as in Fig. 4

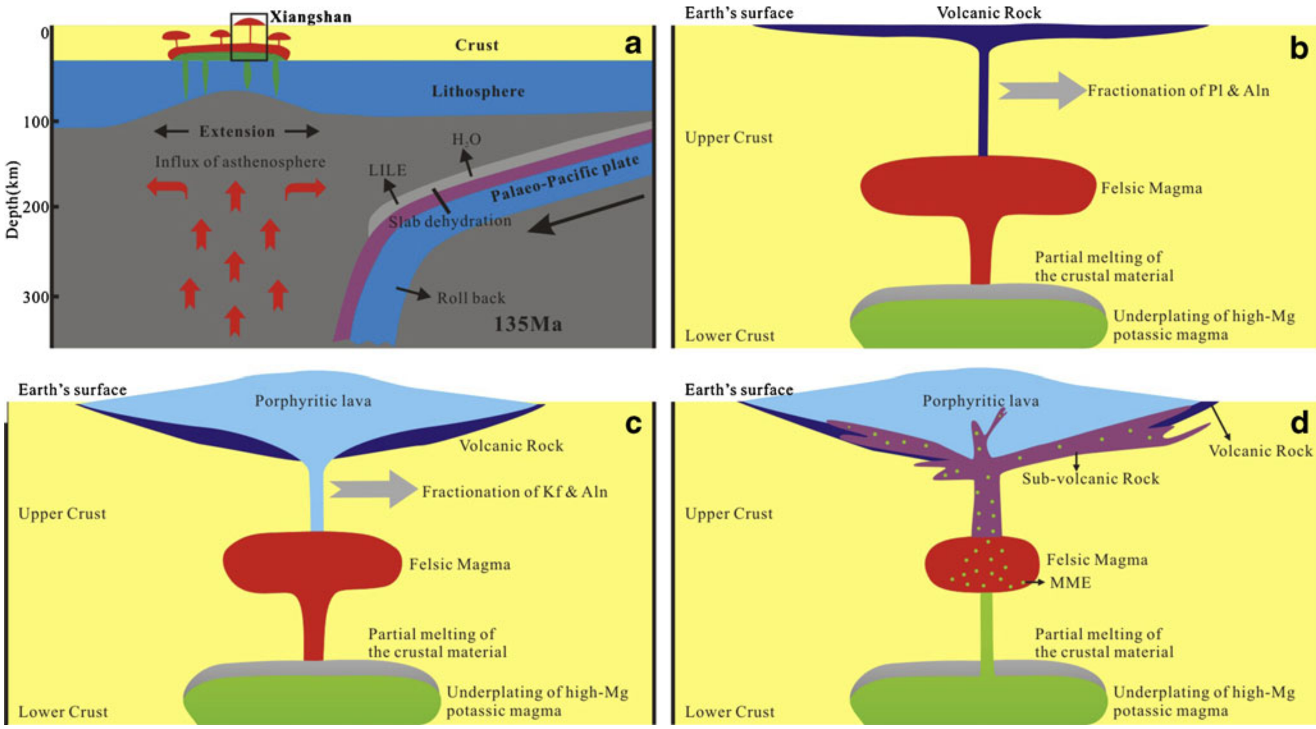

Fig. 12 Schematic diagram showing magma generation processes for the Xianghsan volcanic-intrusive complex and mafic microgranular enclaves. The volcanic-intrusive complex was formed in a continental extensional setting as a consequence of slab roll-back (**a** modified after Jiang et al. 2005). The complex has undergone advanced fractional crystallization with separation of plagioclase, K-feldspar and accessory minerals such as allanite in the crystallization of rhyodacite, rhyodacitic porphyry and porphyroclastic extrusives (**b**, **c**). The formation of the Xiangshan mafic microgranular enclaves can be explained by the injection of the basaltic magma from deep seated magma chamber toward hypabyssal acidic magma chamber at the acidic magma emplacement levels (**d**). See text for more discussion

Acknowledgements The authors are grateful to Dun-Yi Liu, Yu-Ruo Shi and Ke-Jun Hou from Chinese Academy of Geological Sciences for their great help with the lab work of SHRIMP zircon dating and the LA-MC-ICP-MS in situ Hf isotopic analyses. This study is granted by a key project from the Ministry of Education in China (306007). The manuscript benefited from thoughtful suggestions by Prof. Johann G. Raith, Prof. Gary Hemming, and two anonymous reviewers.

References

Andersen T (2002) Correction of common lead in U–Pb analyses that do not report ^{204}Pb. Chem Geol 192:59–79

Belousova EA, Griffin WL, O'Reilly SY, Fisher NI (2002) Igneous zircon: trace element composition as an indicator of source rock type. Contrib Mineral Petrol 143:602–622

Bouvier A, Vervoort JD, Patchett PJ (2008) The Lu–Hf and Sm–Nd isotopic composition of CHUR: Constraints from unequilibrated chondrites and implications for the bulk composition of terrestrial planets. Earth Planet Sci Lett 273:48–57

Boynton WV (1984) Geochemistry of the rare earth elements: meteorite studies. In: Henderson P (ed) Rare earth element geochemistry. Elsevier, New York, pp 63–114

Charvet J, Lapierre H, Yu YW (1994) Geodynamic significance of the Mesozoic volcanism of southeastern China. J SE Asian Earth Sci 9:387–396

Chen XM, Lu JJ, Liu CS, Zhao LZ, Wang DZ, Li HM (1999) Single-grain zircon U–Pb isotopic ages of the volcanic-intrusive complexes in Tonglu and Xiangshan areas. Acta Petrol Sin 15:272–278

Cherniak DJ, Watson EB (2003) Diffusion in Zircon. Rev Mineral Geochem 53:113–143

Cherniak DJ, Hanchar JM, Watson EB (1997) Diffusion of tetravalent cations in zircon. Contrib Mineral Petrol 127:383–390

Chu NC, Taylor RN, Chavagnac V, Nesbitt RW, Boella RM, Milton JA, German CR, Bayon G, Burton K (2002) Hf isotope ratio analysis using multi-collector inductively coupled plasma mass spectrometry: an evaluation of isobaric interference corrections. J Anal Atom Spectrom 17:1567–1574

Compston W, Williams IS, Meyer CE (1984) U–Pb geochronology of zircons from lunar breccia 73217 using a sensitive high mass-resolution ion microprobe. J Geophys Res 89:B525–B534

Compston W, Williams IS, Kirschvink JL, Zhang ZC, Ma GG (1992) Zircon U–Pb ages for the Early Cambrian time-scale. J Geol Soc 149:171–184

Elhlou S, Belousova E, Griffin WL, Pearson NJ, O'Reilly SY (2006) Trace element and isotopic composition of GJ-red zircon standard by laser ablation. Geochim Cosmochim Acta 70:A158

Fan HH, Ling HF, Shen WZ, Wang DZ, Liu CS, Jiang YH (2001a) Nd–Sr–Pb isotope geochemistry of the volcanic-intrusive complex at Xiangshan, Jiangxi province. Acta Petrol Sin 17:395–402

Fan HH, Wang DZ, Liu CS, Zhao LZ, Shen WZ, Ling HF, Duan Y (2001b) Discovery of quenched enclaves in subvolcanic rocks in Xiangshan, Jiangxi Province and its genetic mechanism. Acta Geol Sin 75:64–69

Fan HH, Wang DZ, Shen WZ, Liu CS, Wang X, Ling HF (2005) Formation age of the intermediate-basic dykes and volcanic-intrusive complex in Xiangshan, Jiangxi Province. Geol Rev 51:86–91

Fang XH, Hou WY, Wan GL (1982) Petrographic studies of the volcanic complex in the Xiangshan Caldera. Acta Petrol Mineral Anal 1:1–10

Fujimaki H (1986) Partition coefficients of Hf, Zr, and REE between zircon, apatite, and liquid. Contrib Mineral Petrol 94:42–45

Gao JF, Lu JJ, Lai MY, Lin YP, Pu W (2003) Analysis of trace elements in rock samples using HR-ICP-MS. J Nanjing Univ Nat Sci 39:844–850

Gilder SA, Keller GR, Luo M, Goodell PC (1991) Eastern Asia and the Western Pacific timing and spatial distribution of rifting in China. Tectonophysics 197:225–243

Gilder SA, Gill J, Coe RS, Zhao XX, Liu ZW, Wang GX, Yuan KR, Liu WL, Kuang GD, Wu HR (1996) Isotopic and paleomagnetic constraints on the Mesozoic tectonic evolution of south China. J Geophys Res 101:16137–16154

Goldstein SL, O'Nions RK, Hamilton PJ (1984) A Sm–Nd isotopic study of atmospheric dusts and particulates from major river systems. Earth Planet Sci Lett 70:221–236

Griffin WL, Pearson NJ, Belousova E, Jackson SE, Van Achterbergh E, O'Reilly SY, Shee SR (2000) The Hf isotope composition of cratonic mantle: LAM-MC-ICP-MS analysis of zircon megacrysts in kimberlites. Geochim Cosmochim Acta 64:133–147

Griffin WL, Wang X, Jackson SE, Pearson NJ, O'Reilly SY, Xu XS, Zhou XM (2002) Zircon chemistry and magma mixing, SE China: in-situ analysis of Hf isotopes, Tonglu and Pingtan igneous complexes. Lithos 61:237–269

Hoskin PWO, Black LP (2000) Metamorphic zircon formation by solid-state recrystallization of protolith igneous zircon. J Metamorph Geol 18:423–439

Hou KJ, Li YH, Zou TR, Qu XM, Shi YR, Xie GQ (2007) Laser ablation-MC-ICP-MS technique for Hf isotope microanalysis of zircon and its geological applications. Acta Petrol Sin 23:2595–2604

Hsü KJ, Sun S, Li JL, Chen HH, Pen HP, Sengor AMC (1988) Mesozoic overthrust tectonics in south China. Geology 16:418–421

Hsü KJ, Li JL, Chen HH, Wang QC, Sun S, Şengör AMC (1990) Tectonics of South China: key to understanding West Pacific geology. Tectonophysics 183:9–39

Hu GR, Zhang BT, Yu RL (1999) A study on Sm–Nd and Rb–Sr isochron ages of the central Jiangxi metamorphic belt. Geol Rev 45:129–134

Jackson SE, Pearson NJ, Griffin WL, Belousov EA (2004) The application of laser ablation-inductively coupled plasma-mass spectrometry to in situ U–Pb zircon geochronology. Chem Geol 211:47–69

Jacobsen SB, Wasserburg GJ (1980) Sm–Nd isotopic evolution of chondrites. Earth Planet Sci Lett 50:139–155

Jahn BM, Zhou XH, Li JL (1990) Formation and tectonic evolution of Southeastern China and Taiwan: isotopic and geochemical constraints. Tectonophysics 183:145–160

Jiang YH, Ling HF, Jiang SY, Fan HH, Shen WZ, Ni P (2005) Petrogenesis of a Late Jurassic peraluminous volcanic complex and its high-Mg, potassic, quenched enclaves at Xiangshan, Southeast China. J Petrol 46:1121–1154

Kouchi A, Sunagawa I (1983) Mixing basaltic and dacitic magmas by forced convection. Nature 304:527–528

Lan CY, Jahn BM, Mertzman SA, Wu TW (1996) Subduction-related granitic rocks of Taiwan. J SE Asian Earth Sci 14:11–28

Lapierre H, Jahn BM, Charvet J, Yu YW (1997) Mesozoic felsic arc magmatism and continental olivine tholeiites in Zhejiang Province and their relationship with the tectonic activity in southeastern China. Tectonophysics 274:321–338

Li XH (2000) Cretaceous magmatism and lithospheric extension in Southeast China. J Asian Earth Sci 18:293–305

Li ZX, Li XH (2007) Formation of the 1300-km-wide intracontinental orogen and postorogenic magmatic province in Mesozoic South China: a flat-slab subduction model. Geology 35:179–182

Li XH, Wang YX, Zhao ZH, Chen DF (1998) SHRIMP U–Pb zircon geochronology for amphibolite from the Precambrian basement in SW Zhejiang and NW Fujian Provinces. Geochimica 27:327–334

Li XH, Li ZX, Li WX, Liu Y, Yuan C, Wei GJ, Qi CS (2007) U–Pb zircon, geochemical and Sr–Nd–Hf isotopic constraints on age and origin of Jurassic I- and A-type granites from central Guangdong, SE China: a major igneous event in response to foundering of a subducted flat-slab? Lithos 96:186–204

Liew TC, Hofmann AW (1988) Precambrian crustal components, plutonic associations, plate environment of the Hercynian Fold Belt of central Europe: indications from a Nd and Sr isotopic study. Contrib Mineral Petrol 98:129–138

Liu CS, Chu XJ, Shen WZ, Chen FR, Wang DZ (1992) The diccovery and genetic significance of Al-rich minerals in Mesozoic volcanic rocks of Dongxiang-Xiangshan, Jiangxi Province. Geol Rev 38:157–163

Ludwig KR (2003) ISOPLOT 3.00: a geochronology toolkit for Microsoft Excel. Berkeley Geochronological Center Special Publication, Berkeley

Lugmair GW, Marti K (1978) Lunar initial $^{143}Nd/^{144}Nd$: differential evolution of the lunar crust and mantle. Earth Planet Sci Lett 39:349–357

Mahood G, Hildreth W (1983) Large partition coefficients for trace elements in high-silica rhyolites. Geochim Cosmochim Acta 47:11–30

Maniar PD, Piccoli PM (1989) Tectonic discrimination of granitoids. Geol Soc Am Bull 101:635–643

Martin H, Bonin B, Capdevila R, Jahn BM, Lameyre J, Wang Y (1994) The Kuiqi peralkaline granitic complex (SE China): petrology and geochemistry. J Petrol 35:983–1015

McDonough WF, Sun SS (1995) The composition of the earth. Chem Geol 120:223–253

Morrison GW (1980) Characteristics and tectonic setting of the shoshonite rock association. Lithos 13:97–108

Patchett PJ (1983) Importance of the Lu–Hf isotopic system in studies of planetary chronology and chemical evolution. Geochim Cosmochim Acta 47:81–91

Philpotts JA, Schnetzler CC (1970) Phenocryst-matrix partition coefficients for K, Rb, Sr and Ba, with applications to anorthosite and basalt genesis. Geochim Cosmochim Acta 34:307–322

Pu W, Zhao KD, Ling HF, Jiang SY (2004) High precision Nd isotope measurement by Triton TI Mass Spectrometry. Acta Geosic Sin 25:271–274

Pu W, Gao JF, Zhao KD, Ling HF, Jiang SY (2005) Separation method of Rb–Sr, Sm–Nd using DCTA and HIBA. J Nanjing Univ Nat Sci 41:445–450

Shen WZ, Chen FR, Liu CS, Wang DZ (1992) Isotopic-geochemical characteristics and sources material for two types of volcanic-intrusive complexes in Jiangxi Province. Acta Petrol Sin 8:177–184

Soderlund U, Patchett PJ, Vervoort JD, Isachsen CE (2004) The ^{176}Lu decay constant determined by Lu–Hf and U–Pb isotope systematics of Precambrian mafic intrusions. Earth Planet Sci Lett 219:311–324

Song B, Zhang YH, Liu DY (2002) Introduction to the naissance of SHRIMP and its contribution to isotope geology. J Chin Mass Spectrom Soc 23:58–62
Steiger RH, Jäger E (1977) Subcommission on geochronology: convention on the use of decay constants in geo- and cosmochronology. Earth Planet Sci Lett 36:359–362
Van Achterbergh E, Ryan CG, Jackson SE, Griffin WL (2001) Data reduction software for LA-ICP-MS. In: Sylvester P (ed) Laser-ablation-ICPMS in the earth sciences: principles and applications. Mineralogical Association of Canada, Ottawa, pp 239–243
Vernon RH (1984) Microgranitoid enclaves in granites—globules of hybrid magma quenched in a plutonic environment. Nature 309:438–439
Wang DZ, Liu CS, Shen WZ, Chen FR (1991) Discovery and geological significance of Mesozoic S-type volcanic rock belt in Dongxiang–Xiangshan, Jiangxi Province. Chin Sci Bull 36:1491–1493
Wang DZ, Liu CS, Shen WZ, Chen FR (1993) The contrast between Tonglu I-type and Xiangshan S-type clastoporphyritic lava. Acta Petrol Sin 9:44–54
Whalen JB, Currie KL, Chappell BW (1987) A-type granites: geochemical characteristics, discrimination and petrogenesis. Contrib Mineral Petrol 95:407–419
Whalen JB, Jenner GA, Longstaffe FJ (1996) Geochemical and isotopic (O, Nd, Pb and Sr) constraints on A-type granite petrogenesis based on the Topsails igneous suite, Newfoundland Appalachians. J Petrol 37:1463–1489
Williams IS (1998) U-Th-Pb geochronology by ion microprobe. In: McKibben MA, Shanks III WC, Ridley WI (eds) Applications of microanalytical techniques to understanding mineralizing processes. Economic Geology Pub Co, 1–35
Williams IS, Claesson S (1987) Isotopic evidence for the Precambrian provenance and Caledonian metamorphism of high grade paragneisses from the Seve Nappes. Scandanavia Caledonides: II. ion microprobe zircon U-Th-Pb. Contrib Mineral Petrol 97:205–217
Williams IS, Buick S, Cartwright I (1996) An extended episode of early Mesoproterozoic metamorphic fluid flow in the Reynolds Range, central Australia. J Metamorph Geol 14:29–47
Wu RG (1999) The features of volcanic formation in Ruyiting Profile of Xiangshan. J E China Geol Insti 22:201–208
Wu RG, Yu DG, Zhang SM (2003) Identification of rhyolite-dacite porphyry and its relation to uranium mineralization at Xiangshan uranium ore-field. Uran Geol 19:81–87
Wu FY, Yang YH, Xie LW, Yang JH, Xu P (2006) Hf isotopic compositions of the standard zircons and baddeleyites used in U–Pb geochronology. Chem Geol 234:105–126
Xia LQ, Xia ZC, Zhang C, Clochiatti R, Dardel J, Joron JL (1992) Petrogeochemistry of Mesozoic uraniferous volcanic complex from Xiangshan. Geological Publishing House, Beijing
Yang SY, Jiang SY, Jiang YH, Zhao KD, Fan HH (2010) Zircon U–Pb geochronology, Hf isotope and geological implications of the rhyodacite and rhyodacitic porphyry in Xiangshan, Jiangxi Province. Sci China Earth Sci 53:1411–1426
Yoder HS (1973) Contemporaneous basaltic and rhyolitic magmas. Am Mineral 58:153–171
Yu DG (2001) Prospecting ideas for Mesozoic granite-type, volcanics-type and exocontact-type uranium deposits in South China (I). Uran Geol 17:257–265
Yu XQ, Wu GG, Shu LS, Yan TZ, Zhang D, Di YJ (2006) The Cretaceous tectonism of the Gan-Hang Tectonic Belt, southeastern China. Earth Sci Front 13:31–43
Yuan ZX, Wu LS, Zhang ZQ, Ye XJ (1991) The Sm–Nd, Rb–Sr isotopic age-dating of Mayuan Group in Northern Fujian. Acta Petrol Mineral 10:127–132
Yurimoto H, Duke EF, Papike JJ, Shearer CK (1990) Are discontinuous chondrite-normalized REE patterns in pegmatitic granite systems the results of monazite fractionation? Geochim Cosmochim Acta 54:2141–2145
Zeck HP (1970) An erupted migmatite from Cerro del Hoyazo, SE Spain. Contrib Mineral Petrol 26:225–246
Zhang WL, Li ZY (2007) Single-zircon U–Pb age of rhyodacite from Xiangshan area and its geological implications. Acta Petrol Mineral 26:21–26
Zhou XM, Li WX (2000) Origin of Late Mesozoic igneous rocks in Southeastern China: implications for lithosphere subduction and underplating of mafic magmas. Tectonophysics 326:269–287
Zhou XM, Sun T, Shen WZ, Shu LS, Niu YL (2006) Petrogenesis of Mesozoic granitoids and volcanic rocks in South China: a response to tectonic evolution. Episodes 29:26–33